The Thesis Committee for Derek Alexander Pisner
Certifies that this is the approved version of the following Thesis

Superior Longitudinal Fasciculus Microstructure and its Functional Triple-Network Mechanisms in Depressive Rumination

APPROVED BY
SUPERVISING COMMITTEE:

David Schnyer, Supervisor

Christopher Beevers

Superior Longitudinal Fasciculus Microstructure and its Functional Triple-Network Mechanisms in Depressive Rumination

by

Derek Alexander Pisner

Thesis

Presented to the Faculty of the Graduate School of

The University of Texas at Austin

in Partial Fulfillment

of the Requirements

for the Degree of

Master of Arts

The University of Texas at Austin

December 2018

Dedication

To my family for their bravery.

Acknowledgements

I would first like to thank the technical staff at the Texas Advanced Computing Center for supplying the computational resources that would have otherwise rendered the neuroimaging analyses used for this thesis computationally intractable. I would also like to thank Ryan Hammonds for assistance with data quality control. Finally, I would also like to thank Ari Cohen for her incredible patience and support throughout the drafting of this thesis.

Abstract

Superior Longitudinal Fasciculus Microstructure and its Functional Triple-Network Mechanisms in Depressive Rumination

Derek Alexander Pisner, M.A.

The University of Texas at Austin, 2018

Supervisor: David Schnyer

Depressive rumination, which involves a repetitive focus on one's distress, is associated with function connectivity disturbances of Default-Mode, Salience, and Executive-Control networks, comprising the so-called "triple-network" of attention. Missing, however, is a multimodal account of rumination that neuroanatomically explains the perseveration of these dysfunctional networks as a stable human trait. Using diffusion and functional Magnetic Resonance Imaging, we explored multimodal relationships between rumination severity, white-matter microstructure, and resting-state functional connectivity in N=39 depressed adults, and then directly replicated our findings in a demographically-matched, independent sample (N=39). Among the fully-replicated results, three core findings emerged. First, rumination severity is associated with both disintegrated and desegregated functional connectivity of the triple-network. Second, global microstructural inefficiency of the right Superior Longitudinal Fasciculus (SLF) provides a neuroanatomical connectivity basis for rumination and accounts for anywhere between 25-37% of the variance in rumination (Discovery: p_{corr}<0.01; Replication: p_{corr}<0.01; MSE=0.05). Finally, microstructure of the right SLF and auxiliary white-matter is strongly associated with functional connectivity biomarkers of rumination, both within and between components of the triple-network (Discovery: R^2=0.36, p_{corr}<0.05; Replication: R^2=0.25, p_{corr}<0.05; MSE=0.04-0.06). By cross-validating discovery with replication, our findings advance a reproducible

microstructural-functional brain connectivity model of depressive rumination that unifies neurodevelopmental and neurocognitive perspectives.

Table of Contents

List of Tables

List of Figures

INTRODUCTION

Cognitive models of depression posit that negatively biased self-referential processing plays a critical role in maintaining the disorder[1]. Depressive rumination is the *perseverative* form of this processing that involves a recursive focus on one's symptoms to gain emotional insight that might alleviate those symptoms[2]. In practice, however, this strategy exacerbates depression[3], yielding passive solutions to problems[4], diminished social support[5], and an increased likelihood of post-treatment relapse[6]. Given rumination's toxic influence in depression among other mood disorders[7], both its mechanisms and developmental antecedents have been studied across multiple levels of analysis[7–9]. In the context of neuroimaging, however, this effort has resulted in a heterogeneous set of structural and functional brain biomarkers[10] whose reproducibility and intermodal affinity are mostly unknown[11,12]. The present study therefore aims to identify reproducible structural-functional brain biomarkers of rumination using multimodal neuroimaging with direct replication[7].

A Functional Connectivity Model of Rumination

Although numerous cognitive theories of rumination have been proposed[10,13], empirical evidence from functional neuroimaging has yet to definitively corroborate any one model over another[14]. Common to each of these models however, is a tension among three key mechanisms of rumination that can be summarized alongside their associated resting-state networks (RSN's) as captured with functional Magnetic Resonance Imaging (fMRI)[10,15–17]. These include: (1) disrupted self-referential processing, which broadly encompasses poor metacognition, recursive inner mentation[18,1910], and failures of the Default Mode Network (DMN); (2) negatively-biased thought appraisal, discrepancy detection between self-states and goal-states[20], and poor vigilance[21] titration of the Salience Network (SN)[10,16,22]; and (3) impaired attentional disengagement, which refers to a top-down failure to disengage from negative-biased self-referential processing[23], and is associated with the Executive Control Network (ECN). With this framework as a foundation, we can then use fMRI analysis to describe precise intrinsic alterations of RSN's that relate to each respective rumination mechanism[10,16]. We call this dimension of

analysis *within-network* functional connectivity[10,16]. One study, for instance, found that higher rumination severity is associated with alterations within a Parietal subnetwork of the DMN – the pDMN – that supports reflexive episodic memory refreshing[24–26] and which is uniquely vulnerable to the effects of cognitive resource depletion[15]. Depressed ruminators also more actively engage a Cingulo-Opercular subnetwork of the SN – the coSN – critical for tonic alertness, as well as for maintaining ongoing emotional appraisal of internal cognitive and somatic states[27,28]. Finally, abnormal integration of a prefrontal subnetwork of the ECN – the fECN—might reflect deficits of top-down dysregulation[29] or attentional scope[30] whereby emotionally biased information cannot be easily dispelled from working memory.

Other research has shown, however, that these three mechanisms and their corresponding RSN's do not operate as wholly segregated entities[15,31–33]. In depressed ruminators, for instance, impaired disengagement is thought to amplify and sustain negatively-biased thought appraisal[23,34,35]. When combined with perseveration[11] and reflexive processing, this contaminated appraisal forms a 'vicious cycle' of self-criticism[17,36] which recursively drains cognitive resources needed to disengage from the processing. Because these mechanisms can be mutually reinforcing in this way, their interactivity might further be construed as its own 'metacognitive' dimension of rumination etiology[37,38]. Wells[39] and other theorists have accordingly emphasized a key role for metacognitive beliefs in rumination. Specifically they showed that with respect to treatment, for instance, the personal significance of

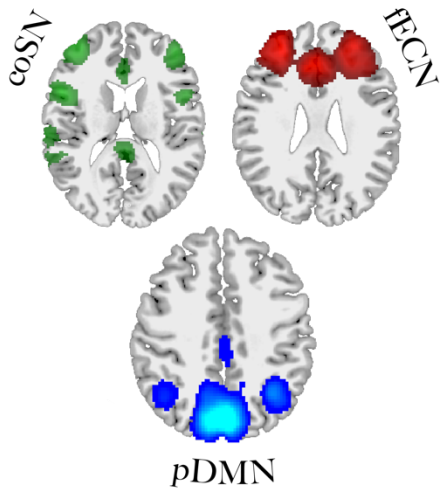

Figure 1: The "triple-network" of attention is a mesoscale system of networks that includes the Salience Network (SN) (*green*), Executive Control Network (ECN) (*red*), and Default Mode Network (DMN) (*blue*), which correspond to three core mechanisms of rumination. Importantly, rumination is known to be correlated with functional connectivity disturbances *within* and *between* these networks.

negative thoughts about rumination and its coping implications may be especially useful targets[40,41]. Perhaps analogous to this metacognitive dimension, interactions among rumination's three core RSN's can also be described on a 'meta-network' basis, where the RSN's themselves are interdependent entities[15,42]. We call this dimension of analysis *between-network* functional connectivity[10,16]. In fact, the DMN, SN, and ECN have been described as belonging to a so-called "triple network" of attention, which some believe to be globally compromised across depression psychopathology[42–45] (*See* **Figure 1**). From this vantage point, Hamilton et al. (2011) showed that the brains of depressed ruminators exhibit greater between-network DMN dominance over the ECN, with a variable role for the SN depending on level of depression severity[46]. In another study, Wang et al. (2016) similarly argued that greater DMN dominance over the ECN, impaired SN–mediated switching between the DMN and ECN, and ineffective ECN modulation of the DMN, each constitute separate cognitive mechanisms of a host of depressive symptoms, including rumination[15].

A Microstructural Connectivity Model of Rumination

In contrast to the cognitive models which describe rumination as a failure of information processing, another line of study has focused on identifying developmental antecedents of rumination; that is, the individual differences that might explain why, unlike other depressive symptoms, rumination uniquely persists as a stable trait. As Papageorgiou once phrased it[39] – "*who becomes a ruminator*"[47]? According to Nolen-Hoeksema's response styles theory (RST), it is those who do not feel in control of their ability to cope and those are helpless to act[47]. By her lights, rumination is a maladaptive *pattern* of responding to distress[3]—a stable individual difference characteristic that she was able to verify over the course of two decades of longitudinal, community-based studies[5]. Although researchers had initially described early environmental risk factors such as dysfunctional parenting and abuse as childhood precursors to rumination[11,39,48], later heritability studies also revealed a prominent role for genetic moderators that largely overlap with those relevant to depression more generally[7]. Nevertheless, the precise *neural* mechanisms whereby genetic and environmental risk factors contribute to

rumination as a stable cognitive trait remain an open question[39]. Not only has this been an impediment to progressing our basic scientific understanding of rumination's underlying mechanisms, it has precluded us from developing more effective, personalized treatments for depression[7,40,49]. Because of this unique developmental risk, moreover, a study that seeks to dually identify *both* cognitive developmental neural biomarkers of rumination in tandem may be uniquely positioned to address this foundational question[50–53].

And in the search for neurodevelopmental biomarkers of rumination, we need not start from scratch. To the extent that resource-intensive, triple-network operations characterize a vicious cycle of negative thoughts that persists repetitively[8,29,54], we should likewise expect structural MRI to be sensitive to grey or white-matter biomarkers capable of scaffolding these operations over time[10,55–57]. Along these lines, some of the earliest voxel-based morphometric studies of depression looked to modular grey matter structures, like the Anterior Cingulate Cortex (ACC), whose thickness or volume explained some variance in rumination severity[55,57,58]. Research into the precise role of ACC volume in rumination has been largely inconsistent, however[10,57,59], perhaps alluding to its dense interconnectivity with other cortical areas[60] or the multiple specialized functions among sub-regions of the ACC itself[61]. Ultimately, appeals made to grey-matter modules alone have become increasingly problematic since they do not capture a commensurate level of complexity to rumination's functional connectivity expression across *distributed* modules[62,63].

The structural analogue to functional connectivity – microstructural connectivity of white-matter[64] – may therefore provide a more flexible framework for conceptualizing the multivariate developmental differences that likely characterize rumination[7]. Perhaps not coincidentally, BOLD signal clustering of resting-state networks produces patterns that spatially resemble white-matter tracts[65]. Microstructural connectivity is typically studied using methods like diffusion Magnetic Resonance Imaging (dMRI), which provides an *in vivo* method for measuring Fractional Anisotropy (FA) based on anisotropic properties of white-matter[66]. Unfortunately, only one study to date has explicitly investigated the microstructural basis for rumination. In 2012, Zuo et al. used

Tract-Based Spatial Statistics (TBSS) to show that FA of the Superior Longitudinal Fasciculus (SLF) and neighboring motor fibers are negatively associated with rumination severity. Due to its nongeneralizable sample size (*N*=15) and reliance on dMRI data alone, however, that study was not positioned to multimodally reconcile these biomarkers with measures of brain function.

A Reproducible Microstructural-Functional Connectivity Model of Rumination

As Schizophrenia studies have recently shown[52,67,68], multimodal analysis can uniquely afford the ability to fuse disparate information across modalities to formulate new ideas that encompass multiple levels of analysis simultaneously. As these few studies have demonstrated, however, the benefits of this approach hinges largely on the experimenter knowing precisely which modalities to use and where, roughly, to look[52]. Although recent studies beyond rumination literature have shown that frontoparietal white-matter, such as the Cingulum (CCG) and the Uncinate Fasciculus (UF), may provide support for DMN [69] and ECN[70], the precise nature of these multimodal associations remains largely unclear[53,68,71]. Hence, more thoroughly delineating these relationships in the context of rumination may be particularly fruitful by elucidating the neurodevelopmental vulnerabilities (i.e. expressed via microstructural connectivity) through which ruminative cognition (i.e. expressed via triple-network functional connectivity) might emerge when exposed to a depressogenic negative thought bias[7,72–75]. While multimodal analysis can greatly increase sensitivity and specificity to disease biomarkers[52,68], this comes at a price. Its multivariate complexity can easily drain degrees of freedom and limit the generalizability of detected effects if not properly balanced by additional effort towards reproducibility[52]. To overcome this obstacle and maximize the translational value of any multimodal findings made[76], our study had two choices; we could either use a massively large sample size (i.e. difficult to obtain in present-day neuroimaging[77]), else perform out-of-sample replication within the same study[78]. Until only recently, this latter possibility would have seemed entirely prohibitive, but the recent rise of open neuroimaging datasets and growth of high-throughput computational analytics[79] has dramatically reduced the burden of labor required to accomplish such a

feat. In the present study, we take this leap. Following initial analysis of a dataset collected at the University of Texas at Austin, we conduct direct replication of our analysis using an independent sample obtained from an open-dataset made publicly available by the Nathaniel Kline Institute[80]. Although the datasets used for our analyses were acquired at different locations, we were able to obtain sub-samples that were coincidentally matched on demographic criteria, contained comparable fMRI and dMRI neuroimaging data, and included equivalent measures of rumination and depression. By exploiting this homogeneity, we were positioned to directly evaluate, regardless of sample size, whether large effects from our Discovery sample generalized to a Replication sample. Those findings that fully replicated would in turn provide a measure of reproducibility beyond statistical power and based on cross-validation[81–86].

We conduct our analyses over three phrases. First, we consider unimodal microstructural and functional connectivity biomarkers of rumination severity so as to replicate and extend findings from prior work. To assure parallel-forms reliability across analytic software and protect against false-positives due to computational error, we further analyze both rsfMRI and dMRI modalities using multiple methodologies[77,87]. The dMRI analyses, for instance, include dual investigations of white-matter microstructure using both Tract-Based Spatial Statistics (TBSS) and global probabilistic tractography methods[66]. Similarly, the rsfMRI analyses include investigations of resting-state functional connectivity, using Dual-Regression[88] and hierarchical network modeling[89] based on Independent Components Analysis (ICA)[16]. For the second phase of analysis, we then assess whether the microstructural and functional connectivity biomarkers of rumination predict one another. Subsequently, we apply the same analytic pipeline used to conduct phases 1-2 of our Discovery analysis to the homogeneously preprocessed, demographically-similar Replication sample. Finally, we cross-validate each fully-replicated regression model to directly quantify test-error and other measures of generalizability.

METHODS

Participants – Discovery sample

Thirty-nine treatment-seeking participants with DSM-IV Major Depressive Disorder (MDD) were recruited for this study from advertisements placed online, in newspapers, and on late night TV. Participants were screened for medical or physical conditions that would preclude participation in an MRI study. They also completed an abbreviated Mini International Neuropsychiatric Interview (MINI)[90] to determine provisional MDD diagnosis, which were then confirmed using in-person Structured Clinical Interviews for the DSM-IV Disorders (SCID)[91]. administered by a trained research assistant. Participants were excluded if they met criteria for past year substance abuse or dependence, current or past psychotic disorder, bipolar disorder, and schizophrenia. Participants receiving pharmacological treatment were allowed into the study if there has been no medication change in the 12 weeks prior to study entry. To minimize brain changes associated with aging, participants were between ages 18-55.

Ethics Statement

The Institutional Review Board at the University of Texas at Austin approved all study procedures and materials and all participants provided signed informed consent.

Depressive Rumination Measurement

The RSQ (Response Styles Questionnaire)[92] is a 10-item self-report measure of the tendency to ruminate. It consists of a total score and two sub-scales: reflection and brooding. The reflection subscale measures an individual's tendency to turn inward to engage in problem-solving and thereby alleviate negative or depressed mood[11], whereas brooding measures the maladaptive form of rumination believed to be a proxy for rumination[11,46]. Brooding specifically reflects the intensity of ruminative responses to expressions of negative emotion[93]. For each item, subjects indicate the frequency of each event on a scale ranging from 0 ("almost never") to 3 ("almost always"), yielding a range of possible scores from 0-30. The brooding subscale has high reliability (α=0.77-0.92)[92], is well-validated within depressed populations[57], decontaminated of any explicitly depressive content[94], and the sub-scale of choice for most studies of rumination in

depression[10,16,23,24,46]. For these reasons, we used the brooding subscale exclusively to measure rumination.

Depression Severity Measurement

The Beck Depression Inventory (BDI)[95] is a 21-item self-reporting questionnaire for evaluating the severity of depression in normal and psychiatric populations. It contains 21 items on a 4-point scale from 0 (symptom absent) to 3 (severe symptoms), and instructs the participant to recall depression symptoms occurring over the previous two weeks.

Imaging Acquisition

MRI scans were acquired on a whole body 3T GE MRI with an 8-channel phase array head coil. The scanning protocol involved collection of a localizer followed by a high-resolution T1 structural scan, two resting state scans of 6 minutes each, a second high-resolution structural scan, and finally a 55-direction diffusion tensor (dMRI) scan. For the resting-state scan, instructions were presented utilizing a back-projection screen located in the MR bore and viewed through a mirror mounted on the top of the head coil. Participants were instructed to remain awake and alert and keep their gaze on a fixation cross (+) presented approximately at the center of their field of view for the 6-minute duration of the scan. (*See* **Appendix, Methods: Section A***).*

dMRI: Preprocessing

Preprocessing of Diffusion Magnetic Resonance Imaging (dMRI) data was carried out using a custom preprocessing workflow that included eddy correction, brain extraction, denoising, and tensor/ball-and-stick model fitting tools adapted from the FMRIB Diffusion Toolbox[96]. To achieve maximal sensitivity and specificity from the dMRI data, preprocessing included rigorous automated and manual quality control steps (*See* **Appendix, Methods: B**).

dMRI: Tract-Based Spatial Statistics (TBSS) and Global Probabilistic Tractography

A number of approaches to dMRI analysis were implemented. To begin, the whole-brain data was interrogated using Tract-Based Spatial Statistics (TBSS)[97] to identify microstructural characteristics that were associated with brooding severity (*See*

Appendix, Methods: Section C). We additionally employed the 'crossing-fibers' extension of TBSS[98], which is less often used due to its computational expense, but can uniquely capture group differences in secondary (i.e. "crossing") fibers, unlike TBSS based on the tensor model alone. For statistical testing, a permutation approach was employed using FSL's "randomise" function with the TFCE Threshold-Free Cluster Enhancement option, generating 10,000 permutations and applying family-wise error (FWE)-correction to obtain cluster inferences. A two-tailed regression model was next generated using FSL's GLM function, whereby RSQ brooding scores were used as the criterion variable with age and gender as nuisance covariates. Age was included due to a well-known confounding influence of age on microstructure [99], and gender was included due to some evidence of gender differences in rumination—namely, that females tend to be more severe ruminators than males[100].

Following TBSS, we sought to corroborate our initial group level, voxel-wise dMRI findings using individual-level tractography, which is an alternative dMRI methodology that attempts to reconstruct known white-matter pathways while retaining each subject's image in native space orientation. Since spatial information is not manipulated in tractography as it is with TBSS [101], tractography could confirm any TBSS findings in native space, while also disconfirming false-positives due to non-physiological factors such as image misalignment, movement, and other factors resulting from the methodological limitations of TBSS[102]. For tractography, we chose to define microstructure as average weighted FA measures from the entire pathways of tracts of interest whose labels included >5 significant voxels from the earlier TBSS stage. These measures were then further analyzed across hemispheres to establish any significant laterality effects[103]. To perform tractography, we specifically used the TRActs Constrained by UnderLying Anatomy (TRACULA) tool in FreeSurfer (version 5.3.0)[66], which delineates 18 known WM bundles in a fully-automated, unbiased manner using each participant's joint dMRI and T1-weighted MRI reconstruction (*See* **Appendix, Methods: Section D**).

rsfMRI Preprocessing

Preprocessing of baseline rsfMRI data was carried out using FSL's FEAT[96], combined with AFNI and FREESURFER tools. Additional control for WM and ventricular CSF confounds was included, and denoising was carried out using FSL's ICA-based Xnoisifier artifact removal tool (FIX) to control for motion and physiological artifact based on an unbiased classifier (*See* **Appendix, Methods: Section E**).

rsfMRI: Dual-Regression and Hierarchical Network Modeling

Group-level Independent Components Analysis (ICA) was performed by employing "temporal concatenation" of the complete, preprocessed rsfMRI time-series from all of the participants and restricted to twenty-five independent component (IC) outputs[104]. Four IC's were manually identified as noise and removed from further examination. Of the remaining twenty-one networks, all were identified using visual inspection by way of reference to the 17 RSN's delineated by the Yeo et al. 2011 atlas[105], thus allowing for identification of the three IC's of the triple-network that were introduced above - the pDMN[24,46], the coSN [43], and the fECN[17,106].-

A dual-regression approach[107] was next performed on the triple-network RSN's, which were used as regressors for each individual subject's 4D set of fMRI volumes in order to extract time-series that were both specific to each subject and to each of the three IC's[64]. Design matrices and contrasts were then created to test for correlations between brooding severity and total average intrinsic connectivity within each of these RSN's, controlling for age and gender. These regression models were tested separately for each RSN, using two-tailed contrasts in an identical manner to that used in TBSS, with FSL's randomise (10,000 permutations) and TFCE cluster-thresholding with whole-brain FWE-correction[108]. To further correct for analysis-level multiple comparisons among the three triple-network RSN's, we also Bonferroni-corrected our alpha significance level for these models to 0.05/3 or p=0.0167.

To investigate interactions between the triple-network RSN's, we utilized FSLNets[38], a MATLAB-based tool that interfaces with FSL. FSLNets treats the group-ICA outputs (generated from the earlier dual-regression stage) as RSN nodes for

hierarchical network modeling[38]. This involved estimating a partial-correlation matrix for each RSN for each participant. To perform between-RSN general linear modeling, randomise was again employed with FWE-correction, but this time using the nets_glm function at 10,000 permutations. The design matrices and contrasts used in the earlier FSL GLM analyses, were used in this analysis as well.

Participants – Replication Sample

To formally test whether the findings would generalize beyond the discovery sample[109], we directly replicated all stages of analysis using a phenotypically similar, independent sample obtained from the publicly-available, multi-site Nathaniel Kline Institute Rockland dataset[80]. By coincidence, that dataset contained a sub-sample of participants with equivalent demographics to those participants from our original sample; this included (*N*=39) participants who were between the ages of 18-55, had no history of drug abuse or severe comorbid psychopathology, had both useable dMRI data and rsfMRI data, and reported at least some depressive symptomatology. The participants had also been administered the 21-item Beck Depression Inventory (BDI-II) and the 22-item Rumination Response Scale (RRS)(*See* **METHODS: Depressive Rumination Measurement**), which contained identical brooding sub-scale items to those administered in the 10-item RSQ scale [94]. As part of a larger battery of measures, many but not all participants also completed the Structured Clinical Interview for DSM-IV-TR Axis I Disorders (SCID)[110]. Specifically, 33% of the n=36 participants met full criteria for MDD (18% current/recurrent and 15% in remission), requiring that the remaining participants be included on the basis of broader depressive symptomology or a history of depression diagnosis. To maximize useable data, we therefore also included 66% with dysphoria as determined by dysphoric elevations (>4)[111,112] in BDI-II scores.

Cross-Validating Discovery

Furthermore, to minimize the possibility of sample-variant effects due to incongruence of neuroimaging acquisition parameters across samples[113], we spatially and temporally resampled the rsfMRI and dMRI data in the replication sample to match the voxel resolution of the rsfMRI and dMRI data and the sampling frequency (i.e. TR) of

the rsfMRI data in the discovery sample (*See* **Appendix, Methods: Sections F & G**). To ensure direct equivalence of neuroimaging data preprocessing in the replication[87], we also applied an equivalent analytic pipeline to that applied to the discovery sample, but using the pDMN, fECN, and coSN group-ICA RSN definitions from the discovery dataset as the input to both dual-regression and FSLnets. Lastly, given the multiple scanner sites used to collect the neuroimaging data in the Replication sample, we employed mixed-effects regression models (both with FSL's GLM and in R 3.4.0), whereby scanner site was additionally modeled as a random effect.

Since generalizability was a core aim of our study, power analyses were also conducted for detecting a large effect size when using multiple regression with two covariates (age and gender)[22,94,114] (*See* **Appendix: Methods, Section H**). Given our sub-optimal sample-sizes, we also opted to filter significant findings by a large effect size cutoff of R^2=0.25 for non-voxel-wise tests (i.e. tractography, multimodal analysis of beta-coefficients) and p<0.01 FWE-corrected threshold for voxel-wise tests (TBSS, Dual-Regression, FSLnets). This step would serve to more stringently identify those findings with the highest putative generalizability as well as those at greatest risk of replication failure. Further, we conservatively classified a finding as being a 'full replication' only if it replicated with respect to both equivalence in directionality of the effect and the RSN's or anatomical location(s) implicated. Likewise, the fully-replicated findings needed to meet our effect-size cutoff in at least one of the two samples and survive a Family-Wise Error (FWE)/False Discovery Rate (FDR)-corrected significance level of α<0.05[115] or α<0.001 uncorrected for ROI analyses[116]. To directly quantify generalizability, we additionally created standardized regression models variations that could in turn be used to predict Mean Squared Error (MSE) across samples. Finally, to evaluate analysis-level false-discovery, we further used a meta-analytic null-distribution based on replication counts (*See* **Appendix: Methods, Section I**).

RESULTS I: DISCOVERY SAMPLE

Descriptive Statistics and Behavioral Findings

Depressive rumination severity (DR) as measured using the RSQ was normally distributed (M= 9.08, SD= 3.01, range: 17-48, IQR=5; Shapiro-Wilk = 0.976, p = 0.53). Depression severity was also normally distributed (M= 31.94, SD= 8.16, range: 1-15, IQR=10, Shapiro-Wilk = 0.976, p = 0.35) and was modestly associated with rumination severity (R^2 = 0.13, $F(1, 37)$ = 5.61, p=0.02). Age was positively skewed (M=27.51, SD = 8.80, range: 18-52) due to an overrepresentation of young adults in our discovery sample. Although age was weakly correlated with RSQ brooding scores (R^2 = 0.09, $F(1, 37)$ = 3.84, p<0.06) and interacted with several neuroimaging measures throughout our analyses, no significant interactions with gender were observed in either discovery or replication samples. Nevertheless, we retained both age and gender as nuisance covariates for each regression model to ensure maximal generalizability and consistency across our analyses.

'Within-Network' Functional Connectivity and Depressive Rumination

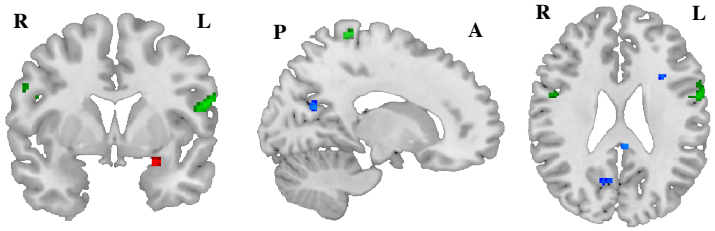

Figure 2: Significant clusters that exhibited lower functional connectivity within the pDMN associated with DR are depicted in blue, and include the PCC, Precuneus, left Precentral Gyrus, left Somatosensory Cortex, and the left inferior Frontal Gyrus. Significant clusters exhibiting lower functional connectivity within the coSN are depicted in green and include the dorsal left Precentral Gyrus, right superior Postcentral gyrus, left inferior Frontal Gyrus, and Broca's area bilaterally. Finally, significant clusters exhibiting greater functional connectivity within the fECN are depicted in red and include the left Amygdala and left Parahippocampal Gyrus.

We next tested whether rumination was associated with resting-state functional connectivity of the three triple-network RSN's as identified from the outputs of group-ICA followed by dual-regression (**METHODS: rsfMRI Group-ICA & Dual-regression**). Results revealed that rumination was highly correlated with functional connectivity in multiple clusters, some of which belonged to each respective triple-

network RSN (i.e. 'intrinsic' connectivity), but also others that were outside of the respective RSN's (i.e. 'extrinsic' connectivity) (*see* **Figure 2**). With respect to the latter, we found that rumination was positively associated with extrinsic connectivity between the frontal Executive Control Network (fECN) and a small cluster (voxels=15) located at a juncture between the left Amygdala and Parahippocampal Gyrus (p<0.05 FWE**;** *see red clusters in* **Figure 2**). Additionally, the Precuneal Default Mode Network (pDMN) exhibited lower extrinsic connectivity with the left somatosensory areas, left Precentral Gyrus and left inferior Frontal Gyrus (p<0.01 FWE; *see blue clusters in* **Figure 2**), but also lower intrinsic functional connectivity between the Precuneus and PCC. Lastly, the Cingulo-Opercular Salience Network (coSN) exhibited lower intrinsic functional connectivity among the dorsal left Precentral Gyrus, left inferior Frontal Gyrus, right superior Postcentral Gyrus, and most prominently in Broca's area bilaterally (p<0.01 FWE ; *see green clusters in* **Figure 2**).

'Between-Network' Functional Connectivity and Depressive Rumination

Based on prior evidence for the role of the pDMN, coSN, and fECN in rumination, we next used FSLnets to explore whether between-network functional connectivity of each pair combination of triple-network RSN's correlated with rumination severity (*see* **METHODS: Between-Network Functional Connectivity**).

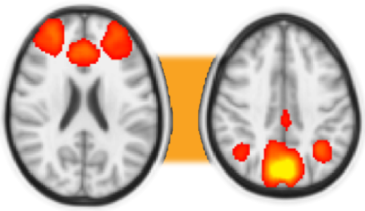

Figure 3: The above image depicts the fECN (*left*) and pDMN (*right*) whose inverse correlation was associated with DR severity (p <0.05 FDR).

That analysis revealed that rumination severity was positively associated with an inverse correlation between the fECN and pDMN (p<0.05 FDR) (*See* **Figure 3**), and between the coSN and the pDMN (p<0.01 FDR). The third 'between-network' correlation (fECN-coSN) was not significantly associated with rumination in the Discovery sample.

Microstructural Connectivity and Rumination

Tract-Based Spatial Statistics (TBSS)

Our next set of analyses sought to identify microstructural biomarkers of rumination. To achieve this, we first employed tensor and crossing-fiber variations of

TBSS (*see* **METHODS: TBSS; Appendix, Methods: Section C**). In association with higher rumination severity, our results first revealed significantly lower FA within large clusters covering the right Superior Longitudinal Fasciculus (SLF, parietal and temporal parts), Cingulum, and Corticospinal Tract (CST) ($p<0.01$ FWE; $p<0.05$ FWE; *see blue FA and green F1 clusters in* **Figure 4**). Some of these clusters also extended into the Anterior Thalamic Radiation (ATR), Uncinate Fasciculus (UF), and Splenium ($p<0.05$ FWE; $p<0.05$ FWE; $p<0.05$ FWE). The crossing-fibers variation of TBSS analysis closely tracked these primary-fiber findings, but further revealed significant correlations with secondary-fibers in a small cluster of the right superior Corona Radiata where the SLFT intersects with the Corpus Callosum at the Centrum Semiovale ($p<0.01$ FWE; *see red cluster in* **Figure 4**).

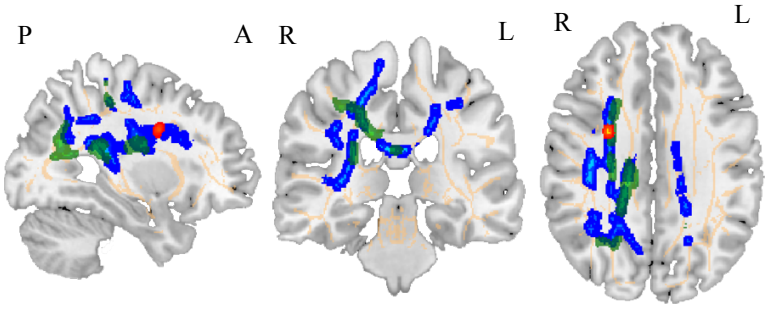

Figure 4: Depressive rumination was associated WM integrity primarily within the temporal and parietal parts of the right SLF including the anterior and posterior Corona Radiata. Surrounding clusters of the right posterior and anterior Cingulum along with bilateral CST also emerged. Here, significant associations with FA ($p<0.01$) are depicted in *blue*, significant associations with the F1 partial volume ($p<0.01$) are depicted in *green*, and significant associations with the F2 "crossing-fibers" volume in the superior at the Corona Radiata ($p<0.01$) are depicted in *red-yellow*. That the FA, F1, and F2 clusters are largely overlapping indicates convergence across deterministic and probabilistic diffusion models, and serves to confirm that detected effects are not the result of model artifact.

Global Probabilistic Tractography

Although TBSS is sensitive to whole-brain white-matter associations, tractography offers greater specificity for labeling known white-matter pathways[66,101]. Because it can be performed in native diffusion space, it is therefore also mostly immune from artifact that might result from the geometric transformations involved in the normalization step in TBSS. Thus, we employed tractography alongside TBSS to ensure parallel-forms reliability. Towards that end, six pathways of interest were automatically

parcellated with tractography and included the SLF, CCG, CST, ATR, UF, and Splenium. As indicated from TBSS, we found a negative association between weighted average FA of the right SLFT and rumination severity (adj. $R^2 = 0.18$, $F(3, 36) = 3.85$, $p_{corrected}<0.005$). This other tracts were not significantly associated with rumination severity.

Tract Hemisphericity

The aforementioned TBSS and tractography analyses indicated that the SLFT WM finding was distinctly right-lateralized. To test this formally, we treated hemisphere as a within-subjects measure and used Analysis of Variance (ANOVA) to compare two GLM's predicting rumination for each tractography measure of global average FA. Specifically, the first GLM used left hemisphere as the predictor, whereas the second GLM used right hemisphere as the predictor, controlling for left hemisphere. From this analysis, we found supportive evidence for right lateralization of the SLFT ($F(36,1)=8.71$, $p=0.005$).

Multimodal Connectivity (Microstructural-Functional) and Rumination

Microstructure Supports 'Within-Network' Functional Connectivity in Rumination

To test for any multimodal relationships between the *within-network* functional connectivity findings and the microstructural connectivity findings, we next extracted the beta coefficients representing average total connectivity intrinsic connectivity for each of the rumination-associated triple-network clusters discovered through dual-regression. This involved creating a matched subsample of $N=32$ subjects, since seven subjects did not have both useable rsfMRI and dMRI data. As an initial step, we extracted beta-coefficients of within-network functional connectivity disruptions in rumination for each subject. Using TBSS, we then regressed these coefficients against whole-brain white-matter on an FWE-

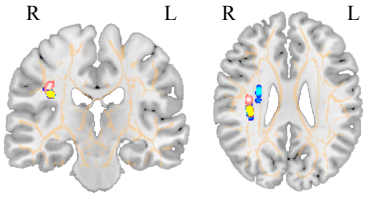

Figure 5) The above slices depict correlations between functional connectivity disruptions of each triple-network component and microstructure of the right SLF. The top row of images depicts a negative correlation between the right medial SLF and the coSN (*pink*) and pDMN (*blue*), along with a positive correlation between the right posterior SLF and the fECN (*yellow*).

corrected voxel-wise basis. The results showed that pDMN and coSN within-network functional connectivity disruptions in rumination were associated with microstructure of both primary and secondary fibers in a right medial SLF cluster (p<0.05, FWE)(*See light blue cluster* **Figure 5**). In contrast, functional connectivity disruptions of the fECN in rumination were *positively* associated with a posterior cluster of the right SLF (*see yellow cluster* **Figure 5**). Using our tractography measure of the right SLFT further substantiated these findings, but only revealed an associated with pDMN within-network functional connectivity (adj. $R^2 = 0.21, F(3, 29) = 3.59, p<0.05$).

Microstructure Supports 'Between-Network' Functional Connectivity in Rumination

We next tested whether microstructural biomarkers of rumination predicted the *between-network* functional connectivity disruptions of the triple-network in rumination. Echoing within-network functional connectivity case, voxel-wise TBSS revealed that a concentrated medial cluster of the right SLFT was positively associated with the between-network inverse correlation of the coSN-pDMN in rumination (p<0.05 FWE, *see red/yellow cluster* **Figure 6**). Diverging from the within-network case, however, TBSS also revealed a positive association between microstructure of the right posterior Corona Radiata (a termination junction of the right posterior SLF) and the coSN-pDMN inverse correlation in rumination (p<0.01 FWE)(*see blue cluster* **Figure 6**). Additionally, microstructure of the left anterior Corona Radiata (a contralateral termination juncture of the left anterior SLF) was negatively associated with the pDMN-fECN inverse correlation in rumination. (p<0.05, FWE) (*see dark red cluster* **Figure 6**). In summary, the between-network functional connectivity disruptions in rumination, as in the within-network case, are consistently associated with SLFT microstructure, but further partially

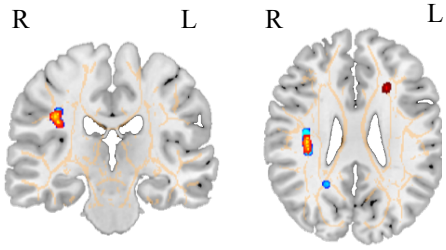

Figure 6): Lower FA of the right medial SLFT and the right posterior Corona Radiata (blue), as well as higher FA of right medial SLFT crossing fibers, was associated with greater pDMN-coSN inverse correlation (red/yellow). Similarly, greater FA of the left anterior Corona Radiata (red) was associated with greater pDMN-fECN inverse correlation.

implicate local microstructure of auxiliary Corona Radiata white-matter. Although the tractography measure of the right SLFT was not significantly associated with between-network functional connectivity when using FA values in FSLnets, cumulative FA of the rumination-associated TBSS mask was positively associated with pDMN-fECN between-network functional connectivity (p<0.05 FDR).

Summary

The initial Discovery sample revealed: 1) Rumination severity is associated with both within-network and between-network functional connectivity alterations of the triple-network; 2) Rumination severity is associated with primary-fiber and secondary-fiber microstructure of the right SLFT, along with localized clusters of auxiliary CCG, CST, ATR, Splenium, and UF white-matter; 3) Microstructure of the right SLFT is multimodally associated with pDMN within-network functional connectivity alterations in rumination; 4) Microstructure of the medial SLFT and anterior/posterior Corona Radiata is associated with between-network functional connectivity of the triple-network. See **Figure 7** for a visual summary of the findings.

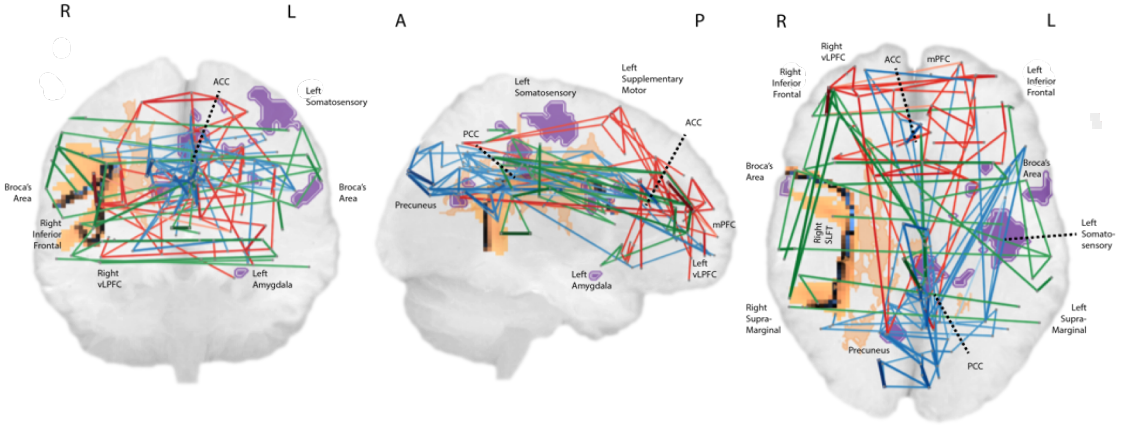

Figure 7): The above multimodal visualization summarizes key microstructural and functional connectivity biomarkers associated with rumination in the discovery sample. WM tracts revealed both by TBSS and tractography are represented in copper heatmap. Regions whose within-network functional connectivity patterns are disrupted in rumination are overlaid in purple. Finally, each of the pDMN, coSN, and fECN as a whole are here depicted as distinct networks with blue, green, and red edge connections, respectively.

RESULTS II: REPLICATION SAMPLE

The Replication sample exhibited similar descriptive statistics to those found in the Discovery sample (*See* **Table 1**). Average rumination severity was similar across samples (M=11.00, SD=2.74, range: 7-20, IQR=2). Age exhibited a slight positive skew (M=31.36, SD = 5.79, Range: 22- 44) as it did in the Discovery sample. Gender distribution was also similar (65% female). Although rumination severity showed a positive skew in the Replication sample, this was corrected using a simple log transformation (Shapiro-Wilk = 0.948, p = 0.07). When applying the analytic methdology used for our Discovery sample to the Replication sample (*See* **METHODS: Replication**), we were able to cross-validate the Discovery findings across all three levels of analysis—1) Triple-network functional connectivity and rumination; 2) Microstructural connectivity and rumination; 3) Multimodal microstructural-functional connectivity and rumination.

Sample Characteristics	Discovery Sample	Replication Sample
Age	M=27.51, SD = 8.80, Range: 18-55	M=31.36, SD = 5.79, Range: 22-44
Gender	22 females (56%)	24 females (65%)
DR Severity	M = 9.08, SD = 3.01	M=11.00, SD=2.74
Depressive Episodes	Moderate-severe MDD diagnosis only	Mild-severe MDD diagnosis, recurrent depression, dysphoria
Depression Severity	M = 31.94, SD = 8.16	M=10.00, SD=6.18
Medication Useage	Permitted if no medication change in the 12 weeks prior to study entry	Permitted if medications were reported as routine. 12-week stability data unavailable.
Other Psychopathology	No severe comorbidity	No severe comorbidity
Scanner Type	Siemens Skyra 3T	Siemens Tim Trio 3T
Multi-site?	No	Yes, 4 separate sites
dMRI parameters	TR/TE=1200/71.1, B=1000, 128 x 128 matrix, 3 mm slice thickness, anistropic voxels, 2 B0 + 53 DWI (55-directions)	TR/TE=2400/85, B=1500, 212 x 212 matrix, 2 mm slice thickness, isotropic voxels, 9 B0 + 128 DWI (137-directions)
rsfMRI parameters	eyes open, TR = 2000 ms, TE = 30 ms, 31 axial slices, voxel size = 3.125 x 3.125 x 3 mm^3 anisotropic	eyes open, TR = 2000 ms, TE = 30 ms, 40 axial slices, voxel size = 3 x 3 x 3 mm^3 isotropic

Table 1: The table above compares key characteristics across Discovery and Replication samples.

Triple-Network Functional Connectivity and Rumination (Replication)

When using a small-volume ROI correction (i.e. MNI atlas-defined masks of significant regions from the discovery sample), the within-network functional connectivity clusters detected from the Discovery sample replicated for each of the pDMN and fECN triple-network components (p<0.001) (*See correspondence of blue and*

red clusters in **Figure 8**). For the pDMN, lower within-network functional connectivity with the right Precuneus fully replicated (p<0.001). Similarly, 9 voxels of the fECN positive connectivity cluster in the left amygdala/ parahippocampal gyrus cluster were overlapping. With respect to between-network functional connectivity, the association between rumination and the pDMN-fECN inverse correlation also fully replicated (p<0.05, FWE).

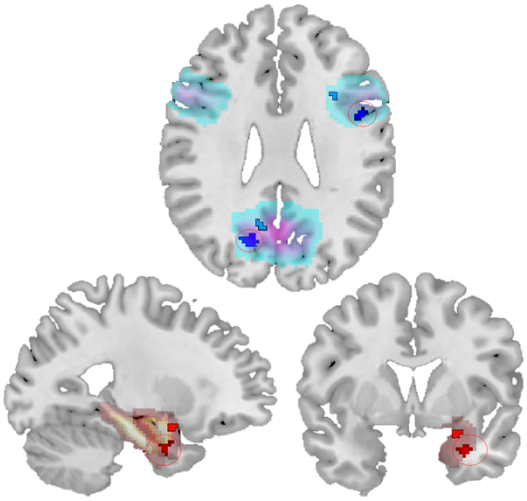

Figure 8: Within-network connectivity findings from the Replication sample (bottom row) compared to those from the Discovery sample (top row). Significant clusters exhibiting lower functional connectivity within the pDMN associated with rumination are depicted in blue. Finally, significant clusters exhibiting greater functional connectivity within the fECN are depicted in red and include the left Amygdala/ parahippocampal Gyrus.

Finally, standardized cross-validated prediction across Discovery and Replication samples revealed an MSE=0.04 for both pDMN and fECN within-network functional connectivity and MSE=0.06 for pDMN-fECN between-network functional connectivity.

Microstructural Connectivity and Rumination (Replication)

The replication yielded a virtually identical set of dMRI findings when applying both TBSS and tractography methods from the Discovery sample to the Replication sample. Using TBSS, we again found that global microstructure of the right SLF, and localized clusters of auxiliary CCG, CST, ATR, Splenium, and UF white-matter were negatively correlated with rumination severity (p<0.05, FWE)(*See* **Figure 9**). At the p=0.05 FWE threshold, 98 voxels, located in the right SLF, CST, and Corpus Callosum (*See top row* **Figure 9**), overlapped in this TBSS analysis across samples. Additionally, replication of the tractography analyses revealed corresponding negative correlations between rumination severity and global microstructure of the right SLFT which, as in the

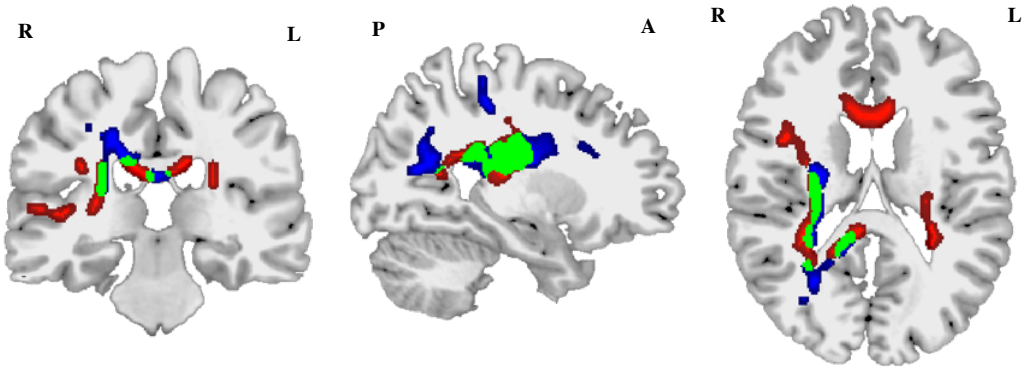

Figure 9: The above mosaic depict TBSS findings from the original sample (blue) and the NKI Rockland replication sample (red). The top row depicts the negative correlations in both samples between rumination and FA (p=0.01 FWE in the discovery sample, p=0.05 FWE in the replication sample). These findings overlapped closely (green) along the right SLF and along the splenium. In the replication sample, there was slightly greater coverage, however, of the genu of the Corpus Callosum.

Discovery sample, was the only association to again survive Bonferroni Correction for the six tracts tested (cond. $R^2 = 0.37$, $F(3, 35) = 8.90$, $p_{corrected}<0.005$). As in the discovery sample, the effect of hemisphere was again significant with respect to the SLFT ($F(36,1)=5.43$, $p=0.03$), affirming that right lateralization of this particular white-matter pathway is a defining feature of rumination. Finally, standardized cross-validated prediction across Discovery and Replication samples revealed an MSE=0.05.

Microstructural-Functional Connectivity (Replication)

Finally, when exploring multimodal microstructural-functional relationships in the replication sample, we again found that global average FA of the right SLFT predicted within-network functional connectivity of the pDMN (*see* **Table 2**)(cond. $R^2 = 0.25$, $p<0.05$, MSE=0.04). Equivalently to the Discovery sample, the positive relationship between WM microstructure and pDMN-fECN between-network functional connectivity was ultimately non-specific to any single tract and implicated the cumulative rumination-associated TBSS clusters, as revealed from FSLnets ($p<0.05$ FDR).

In sum, our results ultimately showed that right SLFT microstructure alone predicted 25-37% of the variance in rumination across discovery and replication samples. Within-network functional connectivity of the pDMN alone also collectively predicted twice as much variance in rumination (52-58%) in both the discovery and replication

samples when controlling for WM microstructure. right SLFT microstructural deficits alone predicted 25-29% of the variance in the pDMN within-network functional connectivity biomarker. Finally, multivariate microstructural deficits across localized clusters of auxiliary tracts like the CCG, CST, ATR, UF, and Corpus Callosum may largely explain the remaining variance in rumination severity and triple-network dysfunction, but future graph analytic studies will be needed to confirm this and non-circularly establish mediation.

Summary of Fully-Replicated Findings

Regression Findings (Predictor and Outcome)	Initial Sample	Replication Sample
Right SLFT Microstructure and Rumination Severity (MSE=0.05)	TBSS ($p<0.01$ FWE, neg) Tractography ($R^2=0.25$, adj. $R^2=0.18$, neg)	TBSS ($p<0.01$ FWE, neg) Tractography (cond. $R^2=0.37$, neg)
pDMN Within-Network Connectivity and Rumination Severity (MSE=0.04)	Dual-regression ($p<0.01$, FWE, neg)	Dual-regression ($p<0.001$, neg)
fECN Within-Network Connectivity and Rumination Severity (MSE=0.04)	Dual-regression ($p<0.01$, FWE, neg)	Dual-regression ($p<0.001$, neg)
pDMN-fECN Between-Network Connectivity and Rumination Severity (MSE=0.06)	FSLnets ($p<0.05$, FDR, neg)	FSLnets ($p<0.01$, FDR, neg)
Right SLFT Microstructure and Rumination-Associated pDMN Within-Network Connectivity (MSE=0.04)	Tractography ($R^2=0.36$, adj. $R^2=0.30$, $p<0.05$, pos) TBSS ($p<0.05$ FWE, pos)	Tractography (cond. $R^2=0.25$, $p<0.05$, pos) TBSS ($p<0.05$ FWE, pos)
Rumination-Associated Cumulative WM microstructure and pDMN-fECN Between-Network Connectivity (MSE=0.06)	FSLnets ($p<0.05$ FDR, pos)	FSLnets ($p<0.05$ FDR, pos)

Table 2: The above table depicts six key findings (*left column*) that directly replicated across the discovery sample (*middle column*) and replication sample (right column), along with Mean-Square Error (MSE) values revealed cross-validation across samples. Each of the middle and right columns states the R^2 value from the respective regression models (adjusted in the discovery sample and conditional on both fixed and random effects in the replication sample), the methodology used to estimate that value (e.g. TBSS, tractography, dual-regression, FSLnets), and the directionality of the relationship (*neg=negative,pos=positive*).

DISCUSSION

Directly replicated across two independent samples, results converged across multiple levels of analysis, revealing reproducible unimodal and multimodal biomarkers of rumination. Apart from differences in depression severity, discovery and replication samples were matched on key behavioral characteristics: both comprised thirty-nine adults with equivalent measures of rumination, similar demographic and inclusion criteria, and comparable neuroimaging acquisition parameters. Using a combination of exploratory regression analysis and cross-validated tests of generalizability, our results firstly showed that self-reported rumination can be explained on the basis of functional disintegration and desegregation among a trio of attentional subnetworks—the Precuneal

Default Mode (pDMN), the Cingulo-Opercular Salience (SN), and the frontal Executive Control (fECN) networks. This initial set of findings served to consolidate known functional connectivity biomarkers of rumination into a cohesive model of multiple neurocognitive mechanisms that echoes prior work[15,31–33,46]. Our findings secondly showed that microstructural differences of the Superior Longitudinal Fasciculus and auxiliary white-matter clusters are robust neurodevelopmental determinants of rumination severity. For the first time, we then unify these dimensions of analysis by demonstrating that rumination-associated functional connectivity alterations of the pDMN specifically (both its within-network and between-network profiles) are largely associated with white-matter microstructure. In essence, our findings advance the notion that depressive rumination is a microstructural-functional connectivity neurophenotype[8,29,54].

A Replicated Triple-Network Functional Connectivity Model of Rumination

Among the fully-replicated findings, we observed several defining within-network functional connectivity features associated with heightened rumination severity. The first of these was disintegration of the right Precuneus within the DMN. This biomarker, which has also been observed in the context of the disorganized thinking characteristic of Schizophrenia[117,118], may reflect uninhibited mind-wandering and autobiographical memory refreshing, along with faulty metacognition[119,120]. Rumination severity was also positively associated with fECN-Amygdala/Parahippocampal connectivity – a finding that may support several mechanisms in depressive rumination[121]. Aligned with existing cognitive models of rumination such as S-REF[39], severe ruminators may perseverate on their own cognitions as a short-term attempt to ward off negative affect, but at the cost of maintaining dysphoric mood in the long term[122]. If rumination were to accordingly operate as though it were adaptive, we might therefore expect it to be accompanied by higher fECN-Amygdala functional connectivity; that is, such a self-regulatory measure might be employed to avoid negative affective states whose discomfort might otherwise serve to contradict the overarching metacognitive belief in rumination's usefulness[123]. Supportively, greater fECN regulation of the Parahippocampal Gyrus could be construed as evidence for suppression of context

from emotionally-charged memories as a means of achieving a subjective sense of recollection during rumination, even if that recollection may in actuality be biased and incomplete[124].

Rumination severity was also consistently negatively associated with a between-network inverse correlation of the pDMN and fECN. This finding in particular underscores a consistent pattern of antagonism between self-referential and cognitive control systems as a defining feature of rumination[15,32,46], but may again reiterate a key role for memory dysfunction in depressive rumination. Since the pDMN is known to be functionally coupled with the hippocampus during memory retrieval[125], greater pDMN-fECN inverse correlation associated with higher rumination severity may reflect a failure to regulate the episodic memory refreshing which occurs naturally during self-referential processing[119]. Conversely, greater pDMN-fECN coupling has been observed during task-related autobiographical planning[32]. Hence, lower pDMN-fECN coupling in the context of rumination might allude to detachment of self-reference from goal-directed cognition[32] or, more broadly, a lack of resting-state metacognition[126]. Our functional connectivity analyses lastly indicated that rumination is associated with between-network and within-network alterations of the coSN, particularly with respect to opercular sections of Broca's Area bilaterally. Echoing findings from prior depression studies[46], however, the precise configuration and directionality of these coSN relationships varied across samples and implied a multivariate pattern of association with rumination that future graph analytic studies with larger sample sizes should be better suited to clarify.

A Replicated Microstructural Connectivity Model of Rumination

Despite the insights into the cognitive mechanisms of depressive rumination afforded by the triple-network functional connectivity model, an exclusive focus on cognitive mechanisms neglects that rumination manifests as a trait-like disposition towards perseverative thinking. To address this dimension more substantially, we next investigated rumination's microstructural biomarkers using dMRI. Those results revealed a diverse set of white-matter clusters distributed throughout the Superior Longitudinal Fasciculus, Cingulum, Corticospinal Tract, Splenium, Uncinate Fasciculus, Anterior

Thalamic Radiation, as well as the Anterior, Posterior, and Superior Corona Radiata. Although these biomarkers cumulatively replicated across samples, tractography revealed that the microstructure of one global white-matter pathway in particular – the Superior Longitudinal Fasciculus (SLF) – could uniquely explain ~31% of the variance in rumination severity on average across samples. Not only did this biomarker replicate with global coverage across the entire tract, it also replicated at Bonferroni corrected thresholds and with consistent right hemispheric lateralization. By employing both tractography and TBSS methodologies in tandem[127], moreover, we were also well-positioned to further explore relevant subdivisions of the SLF[128]. Using tractography, we learned that rumination was globally associated with a portion of the SLF connecting the middle/superior Temporal Gyrus with ipsilateral prefrontal/cingulo-opercular areas. This subdivision is the SLFT, which most closely corresponds to SLF III – also known as the Arcuate Fasciculus. Topographically, the SLFT supplies fiber connections between Wernicke's area for speech production and Broca's area for language comprehension. Compared to other white-matter tracts, SLF microstructure is >50% heritable with <10% variation due to environmental influences of the course of neurodevelopment[129].

Deficits of the right SLFT in rumination may reflect abnormal language systems in the brain. Indeed, bilateral SLFT fibers are believed to broadly facilitate frontoparietal language communication and specifically maintain phonological awareness[130,131]. Research on the microstructural basis of conduction aphasia has accordingly shown that differences in SLFT microstructure may be related to disrupted awareness of speech repetition [132]. As our findings confirmed, rumination-related deficits of the SLFT were distinctly right-lateralized. Although the precise role of the right SLFT is not yet definitive[133], studies have shown that the right SLF in general provides compensatory support for increased demands on language and higher cognitive thought[134,135]. Accordingly, its consistent right lateralization in association with rumination might allude to a distinction between external speech and internal speech. In support of this theory, cortical areas connected by the right SLFT, such as the right Temporoparietal Junction and right superior Temporal Gyrus, have been implicated in internal speech

faculties[10,136,137] and in rumination[58]. Accordingly, we might further speculate that rumination-related differences in right SLFT microstructure might allude to abnormal language repetition patterns of internal monologue[138].

One might also look to Martin's Goal-Progress Theory[139,140] to explain the cerebral lateralization of white-matter deficits associated with rumination severity. By this framework, when depressed individuals do not receive clear, consistent feedback that they are satisfactorily progressing toward their goals, they engage in maladaptive reflection – continuously reformulating poor alternative paths to their goals—over extended periods of time. Put another way, rumination might be construed as an abstraction of the Zeigarnik effect[141] which is the phenomenon whereby incomplete goals tend to remain memory-activated longer than information related to completed goals. To progress towards a goal even in the face of frustrations, individuals need a balance of mental persistence and flexibility, both of which require a continuous supply of cognitive resources[140]. To maintain these activities even in the face of distraction, the left hemisphere broadly provides efficient internal representations consisting of well-established schemas[142]. By comparison, the right hemisphere is largely guided by external contingencies that deviate from existing representations and so allows rumination to operate more flexibly to consider alternative paths to goals[143]. When frontoparietal white-matter of the right hemisphere is therefore broadly deficient, as in the case of global right SLFT microstructural deficits in rumination, it may become more difficult to maintain the ongoing insight needed to reformulate alternative paths. As a result, cognitive flexibility may suffer in the face of the heightened self-goal state discrepancy experienced in depression[140]. Consequently, the problem-solving processes involved in rumination will become resource-depleted, but perseverate notwithstanding because the persistent drive towards goal achievement still remains intact. To our knowledge, our study is the first study to empirically support Martin et al.'s 1989 theory using measures of white-matter microstructure[139].

A Replicated Microstructural-Functional Connectivity Model of Rumination

Although the triple-network functional connectivity model of rumination may provide some insight into *how* ruminative cognition unfolds (i.e. though dysregulated, negatively-biased self-referential processing), it does not offer an account of *why* it occurs recursively or persists as a stable trait. We therefore posit that individual differences in right SLFT microstructure is a robust neurodevelopmental determinant of rumination severity, through the medium of triple-network disorganization, provides the necessary ingredients for depressive rumination. Aligned with this interpretation, our findings showed that microstructure of the right SLFT alone predicted ~26% of the variance in pDMN within-network functional connectivity in both samples. This association in particular implies overlap of the modality-specific roles discussed earlier for the pDMN and right SLFT. Namely, the dysregulated mind-wandering and emotional memory refreshing that perseverates during rumination is closely related to individual differences in resource-availability for supporting cognitive flexibility along with monological language processing. With respect to neurogenetic research of the SLFT, we can infer that these neurodevelopmental differences are predominantly heritable, but likely not immutable[129].

Since white-matter microstructure seemingly did not account for *all* of the variance in rumination-associated triple-network dysfunction, moreover, it is not clear whether this is merely the result of cumulative error variance across modalities or a genuine partial mediation effect. For now, therefore, we suggest that it is insufficient to rely on unimodal microstructural measures alone moving forward. Additionally, the cumulative WM deficits associated with rumination were associated with the between-network pDMN-fECN inverse correlation on a voxel-wise basis in both samples. Still, this latter association was comparatively weaker with some indication of non-linearity that may warrant future studies of 'multilayer' network organization to thoroughly elucidate[144]. For now, however, our findings support the notion that the interface of right SLFT microstructural connectivity and pDMN within-network functional connectivity

captures a crucial and previously unknown feature that appears to support ruminative cognition in depression[7,72–75]

Limitations and Generalizability

By validating our findings with a replication sample, our study contributes the first verifiably generalizable brain model of rumination to the larger corpus of depression literature[82,115]. Likewise, we interpret the relative success of our replication attempt as largely indicative that neuroimaging results are not merely spurious; rather, under conditions of maximal sample homogeneity, reflect verifiably reproducible patterns of brain structure and function associated with behavior. Along these lines, our study informally promotes the idea that out-of-sample direct replication with open-datasets can serve as a powerful tool for ~~cross-~~validating scientific discovery. Namely, we demonstrate through example that replication is not merely a compulsory and risky burden; rather, *it is also a tool* that can help to facilitate reproducible exploration of multimodal hypotheses, and do so with reasonable data economy[77].

One limitation of the present study may be that the neural biomarkers that it uncovered are not purely attributable rumination. Given how closely the theoretical constructs of rumination and depression severity are intertwined, however, there are fundamental theoretical obstacles to establishing specificity of rumination biomarkers to depression[92]. Although the specificity of the Rumination Response Scale to depression is generally assumed[13], it has been challenging to demonstrate, perhaps largely due to the restricted range of rumination severity among non-depressed individuals[8,145]. Nevertheless, participants included in our replication sample were dysphoric and/or depression-remitted, thereby enabling us to at least infer that the replicated rumination biomarkers are reproducibly observable across multiple depressive disorder subtypes and at varying levels of depression severity.

CONCLUSION

In the present study, we aimed to identify joint microstructural and functional connectivity biomarkers of Depressive Rumination, which we achieved in the form of six

fully-replicated multimodal findings across two independent samples. Results from both datasets first supported a functional account of rumination; that is, rumination severity is associated with disorganized patterns of within-network and between-network functional connectivity of the 'triple-network' consisting of the DMN, SN, and ECN. The trio of components that make up this network correspond to each of three distinct, yet interacting mechanisms of rumination pathology—recursive self-referential processing, negatively-biased thought appraisal, and impaired attentional disengagement. Converging across multiple methods of analysis applied to both datasets, our results showed that microstructural dysconnectivity of the right Superior Longitudinal Fasciculus in particular confers a clear vulnerability for rumination as a cognitive trait in the spirit of Nolen-Hoeksema's original Response Styles Theory[47]. Lastly, our multimodal findings begin the process of unifying neurodevelopmental and neurocognitive perspectives of rumination by delineating key multimodal links between microstructural-functional connectivity biomarkers for the first time. It is through this simultaneous consideration of structure and function, moreover, that we might finally begin to answer that nagging question—"*who becomes a ruminator?*". And to stop the rumination, we ask it twice.

Appendix

Methods (*Supplementary)*

Section A: Imaging Acquisition – Initial Sample

Images were collected utilizing whole head coverage with slice orientation to ensure coverage of the whole brain and to reduce artifact (approximately 20 degrees off the AC-PC plane and oriented for best whole head coverage). Participant head motion was minimized by instruction and the use of foam inserts. Functional images were acquired using a GRAPPA parallel imaging EPI sequence that reduces typical EPI distortions and susceptibility artifacts. The T1 structural scans were 3D SPGR volume acquisitions with 1.4 mm sagittal slices for a total of 134 slices (Flip = 10 degrees, repetition time (TR) = 9.7 ms, echo time (TE) = 4 ms, inversion time (TI) = 20 ms, dwell time (TD) = 0 ms, field of view (FOV) = 25 cm, Matrix = 256 x 256, number of repetitions (NEX) = 1). The resting-state scans were acquired with TR = 2000 ms, GRAPPA acceleration factor of two, TE = 30 ms, 31 axial slices, voxel size = 3.125 x 3.125 x 3 mm^3 with a .6 mm inter-slice gap. The dMRI scan consisted of a HARDI (High Angular Resolution Diffusion Imaging) acquisition that was collected using single shot echo planar imaging, and a twice-refocused spin echo pulse sequence, optimized to minimize eddy current-induced distortions (GE 3T, TR/TE=12000/71.1, B=1000, 128x128 matrix, 3 mm (0-mm gap) slice thickness, 2 T2 + 53 DWI). Thirty-seven slices were acquired in the approximate AC-PC plane. The 55 diffusion weighted directions resulted in a high signal-to-noise diffusion volume that took approximately 7 minutes to acquire.

Section B: dMRI Preprocessing

Standard eddy correction was performed using FSL's eddy correction tool with its default options[1]. The b-vectors file was then rotated based on the output of eddy correction to account for the effects of head motion. To control for the potential influence of spurious group differences due to head motion, a motion detection script was employed that uses the output of eddy correction to calculate the mean translation,

rotation, and displacement of image volumes for each subject in x, y, and z dimensions as well as Euclidian space. Following suggestions in recent literature[2], pre-established movement thresholds (0.2° for rotation and 2.0 mm for translation) and semi-automated detection of "venetian blind" signal dropout were used as a basis for rejecting outlier volumes (i.e. directions) within each subject's 4D dataset or the entire subject's dataset if more than 10% of volumes were flagged. Finally, visual quality control was used to ensure that the prior steps accurately captured all major artifacts without flagging false alarms. As a result of these checks, one volume was removed from two participants, two volumes from two participants, and five volumes from one participant. Following the rejection of flagged volumes, nine participants' entire datasets were excluded in total. To additionally improve signal-to-noise ratio (SNR) resulting from prominent Rician and chi-distributed noise in dMRI, NLSAM (Non-Local Spatial and Angular Matching) was used to denoise each DWI dataset[3]. Finally, each of the participants' images were skull-stripped using FSL's Brain Extraction Tool (BET)[4]. Following preprocessing, local "ball-and-stick" modeling of diffusion parameters was performed using FSL's bedpostx tool, which employs Markov Chain Monte Carlo sampling to generate distributions on diffusion parameters at each image voxel in a manner that can also model the impact of crossing fibers[5].

Section C: dMRI Tract-Based Spatial Statistics (TBSS)

In TBSS, all of the participants' native space images are first individually aligned to an FMRIB58_FA standard template using nonlinear registration so as to facilitate voxel-wise estimations of Fractional Anisotropy (FA). Next, the average of the participants' aligned FA maps are used to create a mean FA image, which was then thresholded for FA values ≥ 0.2 to generate a mean FA "skeleton," which represents the centers (maximal FA) of the fiber tracts common amongst the included participants' images. Since TBSS has been shown to be vulnerable to poor image registration[6], a script for registration outlier detection was finally employed to quantitatively evaluate registration quality. This script measures the mean and maximum projection distances across all voxels along each participant's FA skeleton to the mean FA skeleton to search

for any outliers with abnormally high projection distances, which could be indicative of low image quality or poor registration. This quality control step confirmed excellent registration with no FA skeleton outliers among the participants. Following registration, each subject's aligned mean FA, are projected onto the mean FA skeleton for final input into FSL's randomise GLM.

After using the standard tensor model for TBSS to uncover associations with FA of primary fibers, GLM analyses were then repeated using white matter skeleton images of the first and second partial volumes (i.e. "F1" and "F2") generated from bedpostx[5]. This allowed for measurement of secondary fiber pathways such as the Corticospinal Tract and Corpus Callosum, which are known to contain a high density of crossing fibers[7]. The TBSS voxel skeleton approach restricts analysis to only those voxels with a high probability of lying within equivalent white matter pathways in each individual. Next, the mean partial and dyad maps (F1, F2, D1, and D2) from bedpostx were projected onto the mean FA skeleton using tbss_x[8].

Finally, FSL's atlasquery tool was used to estimate white matter tract locations for the significant clusters based on the average probabilities of overlap between significant clusters and probabilistically parcellated white matter regions, as defined by the JHU White-Matter Atlas[9]. To perform exploratory ROI-analysis of white-matter clusters that were only weakly associated with brooding scores, separate masks were created for each JHU atlas label that contained only the DR-associated significant voxels (i.e. at the p=0.05 threshold) belonging to each respective label.

Section D: dMRI Tractography

TRACULA is an algorithm for automated global probabilistic tractography that estimates the posterior probability of 18 major white-matter pathways, given a combination of dMRI and T1-weighted MRI data[10]. In essence, posterior probability estimations are decomposed into a data likelihood function that uses 1) the outputs from bedpostx, along with 2) information about the shape of each pathway derived from prior anatomical knowledge on the pathways according to a set of training participants. The information extracted from these training participants is the probability of each pathway

passing through (or next to) each anatomical segmentation label generated by FreeSurfer[10]. Since this probability is calculated separately for every point along the trajectory of the pathway. Accordingly, there is no assumption that the pathways have the same shape in the study participants and default TRACULA training data, only that the pathways traverse the same regions relative to the surrounding anatomy. The anatomical segmentation labels required by TRACULA were obtained from the automated cortical parcellation and subcortical segmentation outputs from FreeSurfer. Specifically, all T1-weighted anatomical scans from the baseline acquisition (during which the diffusion images we are also acquired) were first processed using recon-all from the FreeSurfer 5.3.0 software package. This processing routine included automated motion correction, removal of non-brain tissue, Talairach transformation, intensity correction, volumetric segmentation, as well as cortical surface reconstruction and parcellation. All reconstructed anatomical images were then inspected for accuracy and minor manual edits were performed as necessary to remove obvious non-brain tissue included within cortical boundaries nearby each subject's WM mask.

Using the cleaned outputs from recon-all, pathway reconstruction was initiated using the trac-all pipeline for TRACULA, after which we further inspected each of the 18 generated tracts for all participants to identify any signs of missing or incomplete tracts. For four participants for whom paths were missing or incomplete, reconstruction was reinitiated using a different random starting point and an additional 'control point' to constrain the tracking. Following this reinitiated tractography stage, data was counted as 'missing' for two participants, for whom the splenium and right ATR tracts, respectively, still failed to reconstruct. Weighted Average Fractional Anisotropy (FA) was then extracted for each tract for each subject for further analysis in Rstudio 3.3.1. This "Weighted Average" measure weighs the average FA values at each voxel weighted by the probability of the tract going through that voxel, and thus provides a more robust, normalized estimate of the expected (mean) value of white-matter microstructure for each tract that is more meaningfully comparable across participants[10].

Section E: rsfMRI Preprocessing

This workflow included brain extraction[4], motion correction[11], spatial smoothing using a Gaussian kernel with a full-width at half maximum (FWHM) of 6 mm, and high-pass temporal filtering with a 100 second cut-off. Functional scans were co-registered to each participant's high-resolution MPRAGE scan using affine linear registration (FLIRT)[11] with twelve degrees of freedom. Finally, conservative white-matter (WM) and ventricular Cerebrospinal Fluid (CSF) masks were generated for each subject using the FREESURFER reconstructions generated for the dMRI tractography analysis. These CSF/WM confound masks, along with motion-detected confounds, were then regressed out of each respective time-series[12]. Each individual rsfMRI dataset was subsequently denoised by performing single-session ICA, followed by hand-labeling of "bad" components" by visual inspection for twenty-five randomly selected participants' datasets[13]. Those hand labeled datasets were then used to train a machine learning classifier. A parallelized version of FSL's ICA-based Xnoiseifier artifact removal tool (FIX)[14] was used with Leave-One-Out cross-validation to derive a study-specific classifier with 96.2% mean accuracy for classifying noise components. That classifier was then iteratively applied to all datasets in order to automatically identify "good" and "bad" independent components (IC's). After identifying all "bad" components, these IC's were in turn stripped from each participant's rsfMRI time-series using fsl_regfilt, which removes structured noise components through regression[14]. Finally, these denoised images were further normalized to an MNI standard space image using linear affine registration with twelve degrees of freedom, in preparation for dual-regression and analysis with FSLnets.

Section F: Imaging Acquisition[15] – Replication Sample

Multimodal MRI data were acquired across four different scanning sites, but on identical scanners (3T Siemens TimTrio) with a 32-channel head coil. We selected rsfMRI data with the shortest TR of 645 ms in the NKI dataset because it yielded the largest analyzable depressed participant pool with RRS scores. The rsfMRI data were collected with an eyes open condition in a single run of about 10 min (900 time points).

Scanning parameters of rs-fMRI data were TE = 30 ms, flip angle = 60°, FOV = 222 × 222 mm^2 , 40 slices and voxel size = 3 mm isotropic. DWI data were collected with TR = 2,400 ms, TE = 85 ms, flip angle = 90°, FOV = 212 × 212 mm^2, 64 slices and voxel size = 2 mm isotropic. The total number of DWI volumes was 137, which included 128 volumes with a b-value of 1,500 s/mm^2 with different gradient directions and 9 interleaved b0 images. Scanning parameters of a T1-weighted structural image were TR = 1,900 ms, TE = 2.52 ms, flip angle= 9°, FOV = 250 × 250 mm^2, 176 slices and voxel size = 1 mm isotropic.

Section G: NKI Rockland Replication

After preprocessing the dMRI data using an equivalent automated workflow to that used in the present study. Unlike the original dMRI data which was a 55-direction HARDI sequence in 1 x 1 x 2 anisotropic voxel resolution, the NKI Rockland dMRI data was acquired using a higher-resolution 137-direction scheme with 2 mm isotropic voxels (*See* **Section F**). In analysis, we proceeded to replicate the TBSS methods, using similar design matrices and contrasts to those used previously albeit with additional columns to control for scanner site as a random effect. FSL's randomise was again used with whole-brain FWE-correction. Finally, we again performed FREESURFER reconstructions of all subjects' T1-weighted anatomical images followed by the fully-automated TRACULA tractography pipeline.

We then proceeded to replicate the rsfMRI methods by preprocessing the rfMRI data using an equivalent semi-automated workflow to that used in the present study. There were some notable modification that needed to be made to facilitate this, however. First, the MRI data from several participants from one of the four scanner sites was acquired in the opposite sagittal direction; for these participants, the images had to be manually flipped (using FSL's fslswapdim) to match the LAS orientation of the other scans in both datasets. Additionally, unlike the original rsfMRI data, the rsfMRI data from the NKI Rockland sample was acquired with 1 mm isotropic voxels at a sub-second TR=0.645 sec (*See* **Section F**), These differences presented several obstacles; first, we could not apply our trained FIX classifier from the original analysis to perform denoising

on the rsfMRI data due to the different acquisition parameters used; second, the different voxel dimensions prevented the re-use of the initial group-ICA triple-network definitions; and third, the sub-second sampling frequency of the Rockland rsfMRI acquisition was three times faster than that used for acquiring the initial rsfMRI data. The latter difference could easily confound any replication attempt since, for example, the SN in particular has been shown to have a different temporal metastability than the ECN and DMN[16]. To remedy these issues, rsfMRI data was temporally-resampled for each participant's time-series by retaining every third volume in each subject's time-series and discarding sub-second volumes so as to yield a TR=1.94 seconds. The resulting datasets were then preprocessed, denoised using their own unique FIX classifier, and normalized to standard space while spatially resampling to 2mm voxels. Regression analyses were performed using corresponding design matrices and contrasts to those used in the original analysis, but as in TBSS, additionally included scanner site with additional columns to control for scanner site as a random effect. Further, dual-regression was performed using a small-volume correction, to only test voxels within each respective triple-network IC and the extrinsic clusters identified from the initial results. Finally, FSLnets analyses were carried out using FWE-correction across only the three 'triple network' group-ICA outputs from the initial dataset.

Section H: Power Analysis

With the available n=39 subjects from the discovery and replications samples, and assuming a minimal large effect size of $R^2 > 0.25$ (i.e. r=0.5), then with two covariates for age and gender, power would be 82.7% at α=0.05, and 60.2% at α=0.01. Thus, large effects observed at α=0.05 would yield power >80% for replication to consider as evidence for or against the null hypotheses.

Section I: Assessing False-Positive Replication Error

Given that our approach uses more researcher degrees of freedom in determining what qualifies as a replication, we sought to disprove the notion that our analytic strategy would enable us to find replication effects in any sample of comparable size. This involved generating a meta-analytic null distribution involved performing 1000 iterations

of the multimodal replication analyses, where each iteration consisted of random permutations of the response values for forty regression models. Upon each permutation, null replications were counted based on whether the replicated hypothesis test (e.g. a mixed-effects regression model) yielded a significant result (p<0.05) according to the power criteria described in **METHODS:** ***Replication and Statistical Power***. Ultimately, this permutation approach yielded a null sampling distribution of replication counts that could be used to infer a 95% confidence interval of false discovery at the meta-analytic level.

REFERENCES (Main)

1. Beevers, C. G. Cognitive vulnerability to depression: A dual process model. *Clinical Psychology Review* **25,** 975–1002 (2005).
2. Lemoult, J. & Joormann, J. Depressive rumination alters cortisol decline in Major Depressive Disorder. *Biol. Psychol.* **100,** 50–55 (2014).
3. Lyubomirsky, S., Layous, K., Bay, E., Chancellor, J. & Nelson-coffey, S. K. Thinking About Rumination : The Scholarly Contributions and Intellectual Legacy of Susan Nolen-Hoeksema. (2015). doi:10.1146/annurev-clinpsy-032814-112733
4. Lyubomirsky, S. in *Rumination: Nature, theory, and treatment of negative thinking in depression* (2003). doi:10.1002/9780470713853.ch2
5. Nolen-Hoeksema, S. & Davis, C. G. 'Thanks for sharing that': Ruminators and their social support networks. *J. Pers. Soc. Psychol.* (1999). doi:10.1037/0022-3514.77.4.801
6. Jacobs, R. H. *et al.* Targeting ruminative thinking in adolescents at risk for depressive relapse: Rumination-focused cognitive behavior therapy in a pilot randomized controlled trial with resting state fMRI. *PLoS One* **11,** (2016).
7. Woody, M. L. & Gibb, B. E. Integrating NIMH Research Domain Criteria (RDoC) into depression research. *Current Opinion in Psychology* **4,** 6–12 (2015).
8. Bagby, R. M., Rector, N. A., Bacchiochi, J. R. & McBride, C. The stability of the response styles questionnaire rumination scale in a sample of patients with major depression. *Cognitive Therapy and Research* **28,** 527–538 (2004).
9. Hankin, B. L. Stability of Cognitive Vulnerabilities to Depression: A Short-Term Prospective Multiwave Study. *J. Abnorm. Psychol.* (2008). doi:10.1037/0021-843X.117.2.324
10. Nejad, A. B., Fossati, P. & Lemogne, C. Self-referential processing, rumination, and cortical midline structures in major depression. *Front. Hum. Neurosci.* **7,** 666 (2013).
11. Nolen-Hoeksema, S., Wisco, B. E. & Lyubomirsky, S. Rethinking Rumination. *Perspect. Psychol. Sci.* **3,** 400–424 (2008).
12. Nolen-Hoeksema, S. The role of rumination in depressive disorders and mixed anxiety/depressive symptoms. *J. Abnorm. Psychol.* **109,** 504–511 (2000).
13. Smith, J. M. & Alloy, L. B. A roadmap to rumination: A review of the definition, assessment, and conceptualization of this multifaceted construct. *Clinical Psychology Review* (2009). doi:10.1016/j.cpr.2008.10.003
14. van Vugt, M. K. & van der Velde, M. How Does Rumination Impact Cognition? A First Mechanistic Model. *Top. Cogn. Sci.* (2018). doi:10.1111/tops.12318
15. Wang, X., Öngür, D., Auerbach, R. P. & Yao, S. Cognitive Vulnerability to Major Depression: View from the Intrinsic Network and Cross-network Interactions. *Harv. Rev. Psychiatry* **24,** 188–201 (2016).

16. Ordaz, S. J. *et al*. Ruminative brooding is associated with salience network coherence in early pubertal youth. *Soc. Cogn. Affect. Neurosci*. nsw133 (2016). doi:10.1093/scan/nsw133
17. Bernstein, E. E., Heeren, A. & McNally, R. J. Unpacking Rumination and Executive Control: A Network Perspective. *Clin. Psychol. Sci*. 216770261770271 (2017). doi:10.1177/2167702617702717
18. Leech, R., Kamourieh, S., Beckmann, C. F. & Sharp, D. J. Fractionating the default mode network: distinct contributions of the ventral and dorsal posterior cingulate cortex to cognitive control. *J. Neurosci*. **31,** 3217–24 (2011).
19. Sheline, Y. I. *et al*. The default mode network and self-referential processes in depression. *Proc. Natl. Acad. Sci. U. S. A*. **106,** 1942–1947 (2009).
20. Menon, V. & Uddin, L. Q. Saliency, switching, attention and control: a network model of insula function. *Brain Struct. Funct*. **214,** 655–667 (2010).
21. Andersen, S. B., Moore, R. A., Venables, L. & Corr, P. J. Electrophysiological correlates of anxious rumination. *Int. J. Psychophysiol*. **71,** 156–169 (2009).
22. Kocsel, N. *et al*. Trait Rumination Influences Neural Correlates of the Anticipation but Not the Consumption Phase of Reward Processing. *Front. Behav. Neurosci*. **11,** (2017).
23. Southworth, F., Grafton, B., MacLeod, C. & Watkins, E. Heightened ruminative disposition is associated with impaired attentional disengagement from negative relative to positive information: support for the "impaired disengagement" hypothesis. *Cogn. Emot*. **31,** 422–434 (2017).
24. Rosenbaum, D. *et al*. Aberrant functional connectivity in depression as an index of state and trait rumination. *Sci. Rep*. **7,** 2174 (2017).
25. Freton, M. *et al*. The eye of the self: Precuneus volume and visual perspective during autobiographical memory retrieval. *Brain Struct. Funct*. (2014). doi:10.1007/s00429-013-0546-2
26. Ahmed, S. *et al*. Association between precuneus volume and autobiographical memory impairment in posterior cortical atrophy: Beyond the visual syndrome. *NeuroImage Clin*. (2018). doi:10.1016/j.nicl.2018.03.008
27. Wu, X. *et al*. Dysfunction of the cingulo-opercular network in first-episode medication-naive patients with major depressive disorder. *J. Affect. Disord*. **200,** 275–283 (2016).
28. Sadaghiani, S. & D'Esposito, M. Functional characterization of the cingulo-opercular network in the maintenance of tonic alertness. *Cereb. Cortex* **25,** 2763–2773 (2015).
29. Mandell, D., Siegle, G. J., Shutt, L., Feldmiller, J. & Thase, M. E. Neural substrates of trait ruminations in depression. *J. Abnorm. Psychol*. **123,** 35–48 (2014).
30. Berman, M. G. *et al*. Neural and behavioral effects of interference resolution in depression and rumination. *Cogn. Affect. Behav. Neurosci*. (2011). doi:10.3758/s13415-010-0014-x
31. Hamilton, J. P., Farmer, M., Fogelman, P. & Gotlib, I. H. Depressive Rumination, the Default-Mode Network, and the Dark Matter of Clinical Neuroscience. *Biological Psychiatry* **78,** 224–230 (2015).
32. Spreng, R. N., Stevens, W. D., Chamberlain, J. P., Gilmore, A. W. & Schacter, D. L. Default network activity, coupled with the frontoparietal control network, supports goal-directed cognition. *Neuroimage* (2010). doi:10.1016/j.neuroimage.2010.06.016
33. Spreng, R. N., Sepulcre, J., Turner, G. R., Stevens, W. D. & Schacter, D. L. Intrinsic Architecture Underlying the Relations among the Default, Dorsal Attention, and Frontoparietal Control Networks of the Human Brain. *J. Cogn. Neurosci*. **25,** 74–86 (2013).
34. Grafton, B., Southworth, F., Watkins, E. R. & MacLeod, C. Stuck in a sad place: Biased attentional disengagement in rumination. *Emotion* **16,** 63–72 (2016).
35. Koster, E. H. W., De Lissnyder, E., Derakshan, N. & De Raedt, R. Understanding depressive rumination from a cognitive science perspective: The impaired disengagement hypothesis. *Clinical Psychology Review* **31,** 138–145 (2011).
36. Brosschot, J. F., Gerin, W. & Thayer, J. F. The perseverative cognition hypothesis: A review of worry, prolonged stress-related physiological activation, and health. *Journal of Psychosomatic Research* (2006). doi:10.1016/j.jpsychores.2005.06.074
37. Clare Kelly, A. M., Uddin, L. Q., Biswal, B. B., Castellanos, F. X. & Milham, M. P. Competition

between functional brain networks mediates behavioral variability. *Neuroimage* **39,** 527–537 (2008).
38. Smith, S. M. *et al*. Functional connectomics from resting-state fMRI. *Trends in Cognitive Sciences* **17,** 666–682 (2013).
39. Papageorgiou, Costas, Wells, A. *Depressive Rumination: Nature, Theory and Treatment*. (John Wiley & Sons, Ltd., 2004).
40. Papageorgiou, C. & Wells, A. Treatment of recurrent major depression with Attention Training. *Cogn. Behav. Pract.* **7,** 407–413 (2000).
41. Wells, A. & Papageorgiou, C. in *Depressive Rumination: Nature, Theory and Treatment* 259–273 (2008). doi:10.1002/9780470713853.ch13
42. Menon, V. Large-scale brain networks and psychopathology: A unifying triple network model. *Trends in Cognitive Sciences* **15,** 483–506 (2011).
43. Wu, X. *et al*. A triple network connectivity study of large-scale brain systems in cognitively normal APOE4 carriers. *Front. Aging Neurosci.* **8,** (2016).
44. Liu, Y. *et al*. Decreased Triple Network Connectivity in Patients with Recent Onset Post-Traumatic Stress Disorder after a Single Prolonged Trauma Exposure. *Sci. Rep.* **7,** (2017).
45. Zheng, H. *et al*. The altered triple networks interaction in depression under resting state based on graph theory. *Biomed Res. Int.* **2015,** (2015).
46. Hamilton, J. P. *et al*. Default-mode and task-positive network activity in major depressive disorder: Implications for adaptive and maladaptive rumination. *Biol. Psychiatry* **70,** 327–333 (2011).
47. Nolen-Hoeksema, S., Morrow, J. & Fredrickson, B. L. Response styles and the duration of episodes of depressed mood. *J. Abnorm. Psychol.* **102,** 20–28 (1993).
48. Watkins, E., Moulds, M. & Mackintosh, B. Comparisons between rumination and worry in a non-clinical population. *Behav. Res. Ther.* **43,** 1577–1585 (2005).
49. Watkins, E. Psychological treatment of depressive rumination. *Current Opinion in Psychology* **4,** 32–36 (2015).
50. O'Halloran, R., Kopell, B. H., Sprooten, E., Goodman, W. K. & Frangou, S. Multimodal neuroimaging-informed clinical applications in neuropsychiatric disorders. *Front. Psychiatry* **7,** 1–14 (2016).
51. Tadayonnejad, R., Yang, S., Kumar, A. & Ajilore, O. Multimodal brain connectivity analysis in unmedicated late-life depression. *PLoS One* **9,** (2014).
52. Calhoun, V. D. & Sui, J. Multimodal Fusion of Brain Imaging Data: A Key to Finding the Missing Link(s) in Complex Mental Illness. *Biological Psychiatry: Cognitive Neuroscience and Neuroimaging* (2016). doi:10.1016/j.bpsc.2015.12.005
53. Uludağ, K. & Roebroeck, A. General overview on the merits of multimodal neuroimaging data fusion. *NeuroImage* (2014). doi:10.1016/j.neuroimage.2014.05.018
54. Fawcett, J. M. *et al*. The origins of repetitive thought in rumination: Separating cognitive style from deficits in inhibitory control over memory. *J. Behav. Ther. Exp. Psychiatry* **47,** 1–8 (2015).
55. Zuo, N. *et al*. White matter abnormalities in major depression: A tract-based spatial statistics and rumination study. *PLoS One* **7,** (2012).
56. Wang, K. *et al*. Individual differences in rumination in healthy and depressive samples: Association with brain structure, functional connectivity and depression. *Psychol. Med.* **45,** 2999–3008 (2015).
57. Kühn, S., Vanderhasselt, M. A., De Raedt, R. & Gallinat, J. Why ruminators won't stop: The structural and resting state correlates of rumination and its relation to depression. *J. Affect. Disord.* **141,** 352–360 (2012).
58. Machino, A. *et al*. Possible involvement of rumination in gray matter abnormalities in persistent symptoms of major depression: an exploratory magnetic resonance imaging voxel-based morphometry study. *J. Affect. Disord.* **168,** 229–235 (2014).
59. Cooney, R. E., Joormann, J., Eugène, F., Dennis, E. L. & Gotlib, I. H. Neural correlates of rumination in depression. *Cogn. Affect. Behav. Neurosci.* **10,** 470–8 (2010).
60. Etkin, a, Egner, T. & Kalisch, R. Emotional processing in anterior cingulate and medial prefrontal. *Trends Cogn. Sci.* **15,** 85–93 (2011).

61. Stevens, F. L., Hurley, R. A. & Taber, K. H. Anterior Cingulate Cortex: Unique Role in Cognition and Emotion. *J. Neuropsychiatry Clin. Neurosci.* **23,** 121–125 (2011).
62. Mazzocchi, F. Complexity and the reductionism-holism debate in systems biology. *Wiley Interdiscip. Rev. Syst. Biol. Med.* (2012). doi:10.1002/wsbm.1181
63. Monnart, A., Kornreich, C., Verbanck, P. & Campanella, S. Just swap out of negative vibes? Rumination and inhibition deficits in major depressive disorder: Data from event-related potentials studies. *Frontiers in Psychology* **7,** (2016).
64. Peer, M., Nitzan, M., Bick, A. S., Levin, N. & Arzy, S. Evidence for Functional Networks within the Human Brain's White Matter. *J. Neurosci.* (2017). doi:10.1523/JNEUROSCI.3872-16.2017
65. Mezer, A., Yovel, Y., Pasternak, O., Gorfine, T. & Assaf, Y. Cluster analysis of resting-state fMRI time series. *Neuroimage* (2009). doi:10.1016/j.neuroimage.2008.12.015
66. Yendiki, A. *et al.* Automated probabilistic reconstruction of white-matter pathways in health and disease using an atlas of the underlying anatomy. *Front. Neuroinform.* **5,** 23 (2011).
67. Sui, J. *et al.* Combination of FMRI-SMRI-EEG data improves discrimination of schizophrenia patients by ensemble feature selection. *2014 36th Annu. Int. Conf. IEEE Eng. Med. Biol. Soc. EMBC 2014* 3889–3892 (2014). doi:10.1109/EMBC.2014.6944473
68. Sui, J., Adali, T., Yu, Q., Chen, J. & Calhoun, V. D. A review of multivariate methods for multimodal fusion of brain imaging data. *Journal of Neuroscience Methods* (2012). doi:10.1016/j.jneumeth.2011.10.031
69. Tao, Y. *et al.* The Structural Connectivity Pattern of the Default Mode Network and Its Association with Memory and Anxiety. *Front. Neuroanat.* **9,** (2015).
70. Steffens, D. C., Taylor, W. D., Denny, K. L., Bergman, S. R. & Wang, L. Structural integrity of the uncinate fasciculus and resting state functional connectivity of the ventral prefrontal cortex in late life depression. *PLoS One* **6,** (2011).
71. Pettersson-Yeo, W. *et al.* An empirical comparison of different approaches for combining multimodal neuroimaging data with support vector machine. *Front. Neurosci.* **8,** (2014).
72. Scott, T. A. Evaluating the response styles theory of depression using descriptive experience sampling. *UNLV Theses/ Diss. Pap.* 124 (2009).
73. Sarin, S., Abela, J. R. Z. & Auerbach, R. P. The response styles theory of depression: A test of specificity and causal mediation. *Cogn. Emot.* **19,** 751–761 (2005).
74. Schmaling, K. B., Dimidjian, S., Katon, W. & Sullivan, M. Response styles among patients with minor depression and dysthymia in primary care. *J. Abnorm. Psychol.* **111,** 350–356 (2002).
75. Hilt, L. M., Armstrong, J. M. & Essex, M. J. Early family context and development of adolescent ruminative style: Moderation by temperament. *Cogn. Emot.* (2012). doi:10.1080/02699931.2011.621932
76. Mulugeta, L. *et al.* Credibility, Replicability, and Reproducibility in Simulation for Biomedicine and Clinical Applications in Neuroscience Credibility in Simulation for Biomedicine and Clinical Applications. **12,** 1–16 (2018).
77. de Haas, B. How to enhance the power to detect brain-behavior correlations with limited resources. *Front. Hum. Neurosci.* **12,** 421 (2018).
78. Button, K. S. *et al.* Power failure: Why small sample size undermines the reliability of neuroscience. *Nat. Rev. Neurosci.* **14,** 365–376 (2013).
79. Gorgolewski, K. J. *et al.* BIDS apps: Improving ease of use, accessibility, and reproducibility of neuroimaging data analysis methods. *PLoS Comput. Biol.* **13,** (2017).
80. Nooner, K. B. *et al.* The NKI-Rockland sample: A model for accelerating the pace of discovery science in psychiatry. *Frontiers in Neuroscience* (2012). doi:10.3389/fnins.2012.00152
81. Cawley, G. C. & Talbot, N. L. C. On Over-fitting in Model Selection and Subsequent Selection Bias in Performance Evaluation. *J. Mach. Learn. Res.* **11,** 2079–2107 (2010).
82. Evans, S. What Has Replication Ever Done for Us? Insights from Neuroimaging of Speech Perception. *Front. Hum. Neurosci.* (2017). doi:10.3389/fnhum.2017.00041
83. Poldrack, R. A. *et al.* Scanning the horizon : towards. *Nat. Publ. Gr.* (2017). doi:10.1038/nrn.2016.167

84. Poldrack, R. A. ScienceDirect Predictive models avoid excessive reductionism in cognitive neuroimaging. 1–6 (2019). doi:10.1016/j.conb.2018.11.002
85. Smith, S. M. & Nichols, T. E. Statistical Challenges in "Big Data" Human Neuroimaging. *Neuron* **97,** 263–268 (2018).
86. Nichols, T. E. Multiple testing corrections, nonparametric methods, and random field theory. *Neuroimage* **62,** 811–815 (2012).
87. Bowring, A., Maumet, C. & Nichols, T. Exploring the Impact of Analysis Software on Task fMRI Results. *bioRxiv* (2018). doi:10.1101/285585
88. Abou Elseoud, A. *et al*. Group-ICA Model Order Highlights Patterns of Functional Brain Connectivity. *Front. Syst. Neurosci.* **5,** 37 (2011).
89. Parlatini, V. *et al*. Functional segregation and integration within fronto-parietal networks. *Neuroimage* **146,** 367–375 (2017).
90. Sheehan, D. V. *et al*. The Mini-International Neuropsychiatric Interview (M.I.N.I.): The development and validation of a structured diagnostic psychiatric interview for DSM-IV and ICD-10. in *Journal of Clinical Psychiatry* **59,** 22–33 (1998).
91. First, M. B. et, Spitzer, R. L., Gibbon, M. & Williams, J. B. W. *Structured Clinical Interview for DSM-IV Axis I Disorders, Clinician Version (SCID-CV). for DSMIV* (1997).
92. Erdur-Bakera, Ö.¨ & Bugaya, A. The short version of ruminative response scale: Reliability, validity and its relation to psychological symptoms. in *Procedia - Social and Behavioral Sciences* **5,** 2178–2181 (2010).
93. Nolen-Hoeksema, S. & Morrow, J. A prospective study of depression and posttraumatic stress symptoms after a natural disaster: the 1989 Loma Prieta Earthquake. *J. Pers. Soc. Psychol.* **61,** 115–121 (1991).
94. Treynor, W., Gonzalez, R. & Nolen-Hoeksema, S. Rumination reconsidered: A psychometric analysis. *Cognit. Ther. Res.* **27,** 247–259 (2003).
95. Beck, A., Steer, R. & Brown, G. Beck Depression Inventory-II. *San Antonio* 12–15 (1996). doi:10.1037/t00742-000
96. Jenkinson, M., Beckmann, C. F., Behrens, T. E. J., Woolrich, M. W. & Smith, S. M. FSL. *NeuroImage* **62,** 782–790 (2012).
97. Smith, S. M. *et al*. Tract-based spatial statistics: Voxelwise analysis of multi-subject diffusion data. *Neuroimage* **31,** 1487–1505 (2006).
98. Jbabdi, S., Behrens, T. E. J. & Smith, S. M. Crossing fibres in tract-based spatial statistics. *Neuroimage* **49,** 249–256 (2010).
99. Westlye, L. T. *et al*. Life-span changes of the human brain white matter: diffusion tensor imaging (DTI) and volumetry. *Cereb. Cortex* **20,** 2055–2068 (2010).
100. Nolen-Hoeksema, S. Sex Differences in Unipolar Depression: Evidence and Theory. *Psychological Bulletin* **101,** 259–282 (1987).
101. De Groot, M. *et al*. Improving alignment in Tract-based spatial statistics: Evaluation and optimization of image registration. *Neuroimage* **76,** 400–411 (2013).
102. Torgerson, C. M. *et al*. DTI tractography and white matter fiber tract characteristics in euthymic bipolar I patients and healthy control subjects. *Brain Imaging Behav.* **7,** 129–139 (2013).
103. Vernooij, M. W. *et al*. Fiber density asymmetry of the arcuate fasciculus in relation to functional hemispheric language lateralization in both right- and left-handed healthy subjects: A combined fMRI and DTI study. *Neuroimage* **35,** 1064–1076 (2007).
104. Beckmann, Mackay, Filippini & Smith. Group comparison of resting-state FMRI data using multi-subject ICA and dual regression. *Neuroimage* **47,** S148 (2009).
105. Thomas Yeo, B. T. *et al*. The organization of the human cerebral cortex estimated by intrinsic functional connectivity. *J. Neurophysiol.* **106,** 1125–1165 (2011).
106. Dutta, A., McKie, S. & Deakin, J. F. W. Resting state networks in major depressive disorder. *Psychiatry Res.* **224,** 139–51 (2014).
107. Smith, S. M. The future of FMRI connectivity. *NeuroImage* **62,** 1257–1266 (2012).
108. Smith, S. M. & Nichols, T. E. Threshold-free cluster enhancement: Addressing problems of

smoothing, threshold dependence and localisation in cluster inference. *Neuroimage* **44,** 83–98 (2009).
109. Poldrack, R. A. *et al*. Scanning the horizon: Towards transparent and reproducible neuroimaging research. *Nat. Rev. Neurosci*. **18,** 115–126 (2017).
110. First, M. B., Gibbon, M., Spitzer, R. L., Gibbon, M. & Williams, J. B. W. in *American Psychiatric Press, Inc*. (1997).
111. Berle, D. & Moulds, M. L. Emotional Reasoning Processes and Dysphoric Mood: Cross-Sectional and Prospective Relationships. *PLoS One* (2013). doi:10.1371/journal.pone.0067359
112. Williams, A. D. & Moulds, M. L. Investigation of the indulgence cycles hypothesis of suppression on experimentally induced visual intrusions in dysphoria. *Behav. Res. Ther*. (2007). doi:10.1016/j.brat.2007.07.001
113. Gouttard, S., Styner, M., Prastawa, M., Piven, J. & Gerig, G. Assessment of reliability of multi-site neuroimaging via traveling phantom study. in *Lecture Notes in Computer Science (including subseries Lecture Notes in Artificial Intelligence and Lecture Notes in Bioinformatics)* (2008). doi:10.1007/978-3-540-85990-1-32
114. Butler, L. D. & Nolen-Hoeksema, S. Gender differences in responses to depressed mood in a college sample. *Sex Roles* **30,** 331–346 (1994).
115. Eklund, A., Nichols, T. E. & Knutsson, H. Cluster failure: Why fMRI inferences for spatial extent have inflated false-positive rates. *Proc. Natl. Acad. Sci*. (2016). doi:10.1073/pnas.1602413113
116. Poldrack, R. A. & Mumford, J. A. Independence in ROI analysis: Where is the voodoo? *Soc. Cogn. Affect. Neurosci*. **4,** 208–213 (2009).
117. Utevsky, A. V., Smith, D. V. & Huettel, S. A. Precuneus Is a Functional Core of the Default-Mode Network. *J. Neurosci*. **34,** 932–940 (2014).
118. Wang, Y. *et al*. Resting-state functional connectivity changes within the default mode network and the salience network after antipsychotic treatment in early-phase schizophrenia. *Neuropsychiatr. Dis. Treat*. (2017). doi:10.2147/NDT.S123598
119. Züst, M. A. *et al*. Hippocampus is place of interaction between unconscious and conscious memories. *PLoS One* **10,** (2015).
120. Klaassens, B. L. *et al*. Diminished Posterior Precuneus Connectivity with the Default Mode Network Differentiates Normal Aging from Alzheimer's Disease. *Front. Aging Neurosci*. **9,** 97 (2017).
121. Watkins, E. & Teasdale, J. D. Rumination and overgeneral memory in depression: Effects of self-focus and analytic thinking. *J. Abnorm. Psychol*. **110,** 353–357 (2001).
122. Watkins, E. & Brown, R. G. Rumination and executive function in depression: an experimental study. *J. Neurol. Neurosurg. Psychiatry* **72,** 400–2 (2002).
123. Cohen, N. *et al*. Using executive control training to suppress amygdala reactivity to aversive information. *Neuroimage* **125,** 1022–1031 (2016).
124. Phelps, E. A. & Sharot, T. How (and why) emotion enhances the subjective sense of recollection. *Curr. Dir. Psychol. Sci*. (2008). doi:10.1111/j.1467-8721.2008.00565.x
125. Huijbers, W., Pennartz, C. M. A., Cabeza, R. & Daselaar, S. M. The hippocampus is coupled with the default network during memory retrieval but not during memory encoding. *PLoS One* **6,** (2011).
126. Allen, M. The balanced mind: the variability of task-unrelated thoughts predicts error monitoring. *Front. Hum. Neurosci*. (2013). doi:10.3389/fnhum.2013.00743
127. Efsun Urgerl, Michael D. DeBellis, Steven R. Hooper, Donald P. Woolley, S. C. & Provenzale, and J. M. Influence of Analysis Technique on Measurement of Diffusion Tensor Imaging Parameters. *AJR Am J Roentgenol*. **200,** W510–W517 (2013).
128. Makris, N. *et al*. Segmentation of subcomponents within the superior longitudinal fascicle in humans: A quantitative, in vivo, DT-MRI study. *Cereb. Cortex* **15,** 854–869 (2005).
129. Gustavson, D. E. *et al*. Predominantly global genetic influences on individual white matter tract microstructure. *Neuroimage* **184,** 871–880 (2019).
130. Jenkins, L. M. *et al*. Shared white matter alterations across emotional disorders: A voxel-based meta-analysis of fractional anisotropy. *NeuroImage Clin*. **12,** 1022–1034 (2016).

131. Oechslin, M. S., Imfeld, A., Loenneker, T., Meyer, M. & Jäncke, L. The plasticity of the superior longitudinal fasciculus as a function of musical expertise: a diffusion tensor imaging study. *Front. Hum. Neurosci.* **3,** 76 (2009).
132. Bernal, B. & Ardila, A. The role of the arcuate fasciculus in conduction aphasia. *Brain* **132,** 2309–2316 (2009).
133. Schmahmann, J. D. *et al.* Association fibre pathways of the brain: Parallel observations from diffusion spectrum imaging and autoradiography. *Brain* (2007). doi:10.1093/brain/awl359
134. Shinoura, N. *et al.* Damage to the right superior longitudinal fasciculus in the inferior parietal lobe plays a role in spatial neglect. *Neuropsychologia* **47,** 2600–2603 (2009).
135. Glasser, M. F. & Rilling, J. K. DTI tractography of the human brain's language pathways. *Cereb. Cortex* **18,** 2471–2482 (2008).
136. Lindell, A. K. In your right mind: Right hemisphere contributions to language processing and production. *Neuropsychol. Rev.* **16,** 131–148 (2006).
137. Geva, S. *et al.* The neural correlates of inner speech defined by voxel-based lesion-symptom mapping. *Brain* **134,** 3071–3082 (2011).
138. Alderson-Day, B. & Fernyhough, C. Inner speech: Development, cognitive functions, phenomenology, and neurobiology. *Psychol. Bull.* **141,** 931–965 (2015).
139. Crinion, J. T. *et al.* Neuroanatomical markers of speaking Chinese. *Hum. Brain Mapp.* **30,** 4108–4115 (2009).
140. Fodor, J. A. *The Language of Thought. Philosophical Books* (1975). doi:10.1016/0093-934X(77)90028-1
141. Martin, L. L. & Tesser, A. in *Unintended thought* (1989).
142. Martin, L. L., Shrira, I. & Startup, H. M. in *Depressive Rumination: Nature, Theory and Treatment* (2008). doi:10.1002/9780470713853.ch8
143. Bluma Zeigarnik. ON FINISHED AND UNFINISHED TASKS. 1–15 (1927).
144. Burgess, C. & Simpson, G. B. Cerebral hemispheric mechanisms in the retrieval of ambiguous word meanings. *Brain Lang.* (1988). doi:10.1016/0093-934X(88)90056-9
145. Beeman, M. J. & Bowden, E. M. The right hemisphere maintains solution-related activation for yet-to-be-solved problems. *Mem. Cogn.* (2000). doi:10.3758/BF03211823
146. Braun, U. *et al.* From Maps to Multi-dimensional Network Mechanisms of Mental Disorders. *Neuron* **97,** 14–31 (2018).
147. Roelofs, J., Muris, P., Huibers, M., Peeters, F. & Arntz, A. On the measurement of rumination: A psychometric evaluation of the ruminative response scale and the rumination on sadness scale in undergraduates. *J. Behav. Ther. Exp. Psychiatry* **37,** 299–313 (2006).

REFERENCES (Appendix)

1. Jones, D. K. *Diffusion MRI. Diffusion MRI* (2009). doi:10.1016/B978-0-12-374709-9.00003-1
2. Yendiki, A., Koldewyn, K., Kakunoori, S., Kanwisher, N. & Fischl, B. Spurious group differences due to head motion in a diffusion MRI study. *Neuroimage* **88,** 79–90 (2014).
3. St-Jean, S., Coupe, P. & Descoteaux, M. Non Local Spatial and Angular Matching: Enabling higher spatial resolution diffusion MRI datasets through adaptive denoising. *Med. Image Anal.* **32,** 115–130 (2016).
4. Smith, S. M. *BET: Brain Extraction Tool. Review: Literature and Arts of the Americas* **39,** (2006).
5. Behrens, T. E. J., Berg, H. J., Jbabdi, S., Rushworth, M. F. S. & Woolrich, M. W. Probabilistic diffusion tractography with multiple fibre orientations: What can we gain? *Neuroimage* **34,** 144–155 (2007).
6. De Groot, M. *et al.* Improving alignment in Tract-based spatial statistics: Evaluation and optimization of image registration. *Neuroimage* **76,** 400–411 (2013).
7. Yeatman, J. D., Dougherty, R. F., Myall, N. J., Wandell, B. A. & Feldman, H. M. Tract Profiles of White Matter Properties: Automating Fiber-Tract Quantification. *PLoS One* **7,** (2012).
8. Jbabdi, S., Behrens, T. E. J. & Smith, S. M. Crossing fibres in tract-based spatial statistics.

Neuroimage **49,** 249–256 (2010).
9. Wakana, S., Jiang, H., Nagae-Poetscher, L. M., van Zijl, P. C. M. & Mori, S. Fiber tract-based atlas of human white matter anatomy. *Radiology* **230,** 77–87 (2004).
10. Yendiki, A. *et al.* Automated probabilistic reconstruction of white-matter pathways in health and disease using an atlas of the underlying anatomy. *Front. Neuroinform.* **5,** 23 (2011).
11. Jenkinson, M., Bannister, P., Brady, M. & Smith, S. Improved optimization for the robust and accurate linear registration and motion correction of brain images. *Neuroimage* **17,** 825–841 (2002).
12. Murphy, K., Birn, R. M. & Bandettini, P. A. Resting-state fMRI confounds and cleanup. *Neuroimage* **80,** 349–359 (2013).
13. Griffanti, L. *et al.* ICA-based artefact removal and accelerated fMRI acquisition for improved resting state network imaging. *Neuroimage* **95,** 232–247 (2014).
14. Salimi-Khorshidi, G. *et al.* Automatic denoising of functional MRI data: Combining independent component analysis and hierarchical fusion of classifiers. *Neuroimage* **90,** 449–468 (2014).
15. Fukushima, M. *et al.* Structure-function relationships during segregated and integrated network states of human brain functional connectivity. *Brain Struct. Funct.* (2017). doi:10.1007/s00429-017-1539-3
16. Lee, W. H. & Frangou, S. Linking functional connectivity and dynamic properties of resting-state networks. *Sci. Rep.* **7,** (2017).
17. Van Aert, R. C. M. & Van Assen, M. A. L. M. Bayesian evaluation of effect size after replicating an original study. *PLoS One* (2017). doi:10.1371/journal.pone.0175302